Size-dependent effects of Ge addition on the coking and sintering tendency of Pt_nGe_x/alumina (n=4,7,11) model catalysts

Guangjing Li,[1] Shawn Chiu,[2] Harry W. T. Morgan,[2] Autumn T. Fuchs,[1] Avital Isakov,[2] Patricia Poths,[2] Zisheng Zhang,[2] Anastassia N. Alexandrova,[2,*] and Scott L. Anderson[1,*,†]

[1]Department of Chemistry, University of Utah, 315 S. 1400 E., Salt Lake City, UT 84112

[2]Department of Chemistry and Biochemistry, University of California, Los Angeles, Los Angeles, California 90095

Abstract

The reactivity and adsorbate binding properties of alumina-supported Pt_n and Pt_nGe_m (n/m = 4/1, 7/2, 11/4) model catalysts were studied using a combination of ethylene and CO temperature-programmed desorption (TPD), He^+ ion scattering (ISS), and detailed density functional theory (DFT). The Pt_n/alumina catalysts gradually deactivated in repeated CO TPD runs and deactivated more rapidly in repeated ethylene TPD runs due to the effects of sintering and carbon deposition (coking). Pt_nGe_m/alumina catalysts were dramatically more stable against deactivation by both sintering and coking. Carbon addition to Pt_n/alumina also increased stability against sintering, but not coking. Ion scattering was used to probe the nature of adsorbate binding, including the effects of both carbon and Ge addition on the accessibility of strong Pt-associated binding sites for ethylene and CO. DFT was used to examine the electronic and geometric structures and ethylene and CO binding properties of Pt_n (n = 4, 7) with added Ge, carbon, or both. Consistent with the ISS results, DFT shows that loss of strong adsorbate binding sites mostly resulted from changes to the electronic properties of the clusters, rather than simple blocking of binding sites by Ge or carbon.

*Senior Author †Corresponding Author

I. Introduction

Catalysts with sub-nano cluster active sites potentially have high mass activity (activity/gram metal) because most or all the cluster atoms are exposed and accessible to reactants. In addition, clusters have physical and chemical properties that can be tuned by varying cluster size, including size-dependent electronic structure and fluxionality (i.e., easy interconversion between isomers) that may enable unique catalysis mechanisms.[1-10] Using small clusters in catalysts has practical problems, however, including a propensity toward sintering or ripening increasing the cluster size, and the possibility of poisoning by adsorbates that may modify the cluster electronic properties or block reactant binding sites. In particular, carbon deposition (coking) under hydrocarbon-rich conditions is a degradation mechanism that affects many catalysts, and for sub-nano clusters the high temperatures where coking tends to occur also are likely to drive sintering. The focus of this study is understanding the mechanisms by which Ge addition stabilizes sub-nano Pt clusters against both sintering and coking when the clusters are saturated by a model alkene (ethylene), and heated.

We previously examined deactivation of sub-nano Pt_n/alumina (n = 4,7,8) and Pt_n/silica (n = 4,7) model catalysts by a combination of sintering and coking, during repeated ethylene temperature-programmed desorption (TPD) experiments. Density functional theory (DFT) with PBE functional[11] and PAW pseudopotentials[12] was used to examine ethylene binding and its effects on cluster structure, stability, and fluxionality.[13, 14] The clusters were found to deactivate rapidly, as shown by the loss of strong ethylene chemisorption sites, with effects from both carbon deposition and sintering. In addition, sintering was found to be size-dependent for Pt_n/alumina, with Pt_4 and Pt_7 showing enhanced (but still imperfect) stability at temperatures to 750 K, compared to neighboring cluster sizes.[15]

In those experiments, sintering was inferred from changes in both numbers of exposed Pt

binding sites estimated by TPD, and in the fraction of Pt atoms in the surface layer, estimated by He^+ ion scattering (ISS). Imaging would provide a more direct way of observing sintering but supports such as the alumina/Ta(110) used here are too thick for transmission electron microscopy (TEM). We have reported scanning TEM (STEM) imaging of Pt_n deposited in UHV on carbon and alumina thin film TEM grids.[16] The STEM was not aberration corrected, but the cluster spot sizes, densities, and stability in repeated scans suggested that the air-exposed Pt clusters were at least reasonably stable under the e-beam at room temperature, but we were not able to test the effects of heating. The relevance of these measurements to sintering on a different support under the effects of heating and/or adsorbate binding and desorption is unclear, thus the present work also relies on TPD and ISS to provide *in situ* probes of sintering.

We also tested the effects of selectively adding boron or tin atoms to the clusters,[13, 14, 17-21] and found that both additives strongly suppressed carbon deposition and also appeared to enhance stability with respect to thermal sintering. Neither boron nor tin was ideal, however. Boron addition suppressed coking but did so by weakening the ethylene binding so much that that it all simply desorbed at low temperatures, and the loss of strong chemisorption sites would likely make the clusters useless for catalysis of reactions such as alkane-to-alkene conversion. Tin addition stabilized the clusters against coking and sintering, however, because the Sn:Pt stoichiometry was high, the numbers of strong chemisorption sites *per* cluster, while stable, were substantially smaller than for equivalent size Pt_n clusters.

Based on DFT results suggesting that Ge should be an interesting dopant,[22] we carried out a detailed study of a prototype Ge-doped Pt cluster catalyst: Pt_4Ge/alumina.[16, 23] This cluster was found to have high stability in repeated ethylene TPD experiments, with good retention of strong ethylene

binding sites, however, the stabilization mechanism was unusual. Ge addition only partially suppressed carbon deposition, however, the amount of carbon *per* cluster self-limited at 2 C atoms/cluster, and DFT showed that the resulting Pt_4GeC_2 clusters were highly stable, yet retained a substantial number of strong chemisorption sites. The obvious question is whether this mechanism might also stabilize the activity of Pt_nGe_m clusters of different sizes and compositions.

This paper reports experiments and theory on larger Pt_nGe_m/alumina cluster sizes, addressing questions such as: Does Ge addition suppress carbon deposition, and if so, how? Is coking self-limiting for the larger clusters, and if so, how does coking vary with cluster size? Does Ge confer stability against both carbon deposition and sintering, and if so, how? Do the effects of Ge (and carbon) addition largely result from simple site blocking, from changes in the Pt electronic properties, or both? These issues were probed by a combination of ethylene and CO TPD, time- and temperature-dependent He^+ ion scattering, and detailed DFT modeling of Pt_n/alumina, Pt_nGe_m/alumina, and $Pt_nGe_mC_2$/alumina samples. Several minor improvements to the experimental protocols were made in the course of this work, aimed at reducing complications from adventitious adsorbates and improving the calibration of the numbers of molecules desorbing in the TPD experiments. Thus, in addition to the new experiments, we repeated previously published[13, 16] C_2D_4 TPD experiments for Pt_4/alumina, Pt_7/alumina, and Pt_4Ge/alumina. For these clusters, the desorption temperature dependences were essentially identical in the old and new results, however, the improved calibration reduced the absolute numbers of D_2 molecules desorbing by ~30% in the new experiments. Although that is within our estimated 50% absolute uncertainty, the new results are reported below so that direct comparisons can be made for different cluster sizes and compositions.

Before presenting the results, we briefly review the literature for ethylene

adsorption/decomposition on Pt and Pt alloy surfaces to provide context. Ethylene binding and hydrogenation/dehydrogenation reactions on well-defined Pt surfaces have been well studied, and for brevity we focus on just a subset of particularly relevant work. At low temperatures ethylene adsorbs in a di-σ arrangement on Pt(111)[24-26] and Pt(100)[27], but forms π-bonds to lower-coordination Pt atoms on surfaces like Pt(210) and Pt(110).[28] For high coverages on Pt(111), desorption of intact ethylene starts at 235 K, but as desorption creates empty sites, the remaining ethylene decomposes, resulting in some ethane desorption at ~285 K, but with most of the decomposition resulting in H_2 desorption with carbon deposition.[29] TPD of C_2D_4 and C_2H_4 co-adsorbed on Pt(111) yielded mixed species like C_2D_3H and C_2H_3D, indicating that recombinative desorption of dissociatively chemisorbed ethylene also contributes to the "intact" ethylene desorption signal.[30] Dehydrogenation proceeds through various intermediates, including ethylidyne ($-CCH_3$),[31-35], which undergoes further dehydrogenation to H_2 plus adsorbed carbon, going to completion by ~ 700 K. For Pt(210), some π-bound ethylene desorbs intact at ~ 250 K, but most dehydrogenates, ultimately resulting in H_2 desorption above ~300 K, again going to completion by ~700 K. For π-bound ethylene on Pt(110)-(1x1), desorption of some methane and H_2 was also observed between 270 and 330 K, but most of the carbon deposited, liberating H_2 below 700 K. For alumina-supported Pt nanoparticles, ethylene was found to adsorb below 180 K as a combination of π-bound ethylene, di-σ bound ethylene, and ethylidyne.[36] The π-bound ethylene desorbed intact below 300 K, while the di-σ ethylene decomposed at higher temperatures, generating H_2 and depositing carbon.

These studies suggest several points that may also apply to sub-nano Pt_n on alumina. Because the TPD experiments below all started with the samples saturated with ethylene, the bulk Pt TPD behavior[26] suggests that we might expect the initial desorption to be dominated by intact ethylene, but

that as desorption creates empty sites, the remaining molecules should tend to decompose, with hydrogen desorbing and carbon depositing. Furthermore, our previous DFT work for C_2H_x bound to Pt_n/alumina[23] showed that C-C bond scission occurred only after dehydrogenation with hydrogen loss, resulting in bound acetylene, which further decomposed yielding 2 C, with the hydrogen desorbing. In addition, the previous studies suggest a correlation between ethylene bonding configuration (di-σ vs. π) and its reactivity.[33, 35, 37-40] Ethylene in π-bonded, sp^2 configurations tended to desorb intact (or hydrogenate if H_2 was co-adsorbed), while di-σ bonded, sp^3 ethylene tended to decompose, depositing carbon and liberating hydrogen. For our system, no hydrogen was added and no hydrogenation products were observed, thus the correlation would be decomposition from di-σ bonded ethylene, v.s. intact desorption of π-bonded ethylene.

Alloying Pt with a second metal (i.e., Co, Cu, Ga, Mn, Sn and Zn) forming bimetallic catalysts, has proven to be effective in enhancing catalyst selectivity and activity in alkane dehydrogenation, often by inhibiting catalyst deactivation via coke formation.[41-51] Only a few studies of PtGe alloy catalysts have been reported, however,[52-54] thus the results below, in addition to probing the effects of Ge addition on sub-nano clusters, may provide insights useful in nano-catalysis as well.

II. Results and Discussion

Details of the experimental and computational methods are given below. Additional detail regarding the preparation of size- and composition-selected Pt_n/alumina and Pt_nGe_m/alumina model catalysts is given in the ***Supporting Information***, along with X-ray photoelectron spectral (XPS) characterization of the Pt:Ge stoichiometry. In short, a Ta(110) single crystal was cleaned by heating to 2100 K in UHV, then a ~4 nm thick alumina film was grown by Al vapor deposition in an O_2 atmosphere, as described previously.[55-57] Size-selected Pt_n were soft-landed on the alumina film to

produce Pt_n/alumina with coverage equivalent to 1.5 x 10^{14} Pt atoms/cm^2 ≈ 0.1 ML. All samples, thus, had identical amounts of Pt, deposited in the form of different size clusters. To prepare Pt_nGe_m/alumina, freshly-prepared Pt_n/alumina samples were exposed at 300 K to ~60 L of $GeCl_4$, followed by ~6000 L of H_2 (leading to HCl loss), and then briefly heated to desorb residual H and Cl as HCl and H_2. The Pt:Ge stoichiometries produced by this process were determined by XPS, as described in the Supporting Information. XPS analysis showed that Ge deposited on Pt sites with efficiency 6 to 10 times higher than on alumina sites, but because 90% of the surface is alumina, there was also Ge present in alumina sites, amounting to ~4% of a close-packed Ge monolayer. As shown below, however, these alumina-bound Ge atoms had little effect on reactivity, compared to Ge bound to the clusters. Note that the Ge deposition process is self-limiting, i.e., doubling the $GeCl_4$ exposure did not significantly increase the amount of Ge deposited, implying that the process was limited by the number of $GeCl_4$ adsorption sites. For this reason, we propose that the clusters have well-defined Pt:Ge stoichiometry, rather than the distribution of Ge doping levels that would have resulted from non-self-limiting deposition.

A. Coking and thermal stability during ethylene temperature-programmed desorption (TPD)

1. Pt_n/alumina:

The binding and reactivity properties of Pt_n/alumina (n = 4, 7, 11) model catalysts were studied by ethylene temperature-programmed desorption (TPD), using C_2D_4 to avoid high background for the hydrogen-desorption channel. Select experiments with C_2H_4 were used to show that there was no significant acetylene desorption. As noted above, new experiments for Pt_n/alumina (n = 4, 7) were done so that Fig. 1 and the tables summarizing the analysis could be based on data taken under conditions identical to those used for Pt_{11} and for the Pt_nGe_m clusters discussed below.

Six sequential TPD experiments were run on each sample to allow observation of changes in

properties, each starting with a saturation dose (~10 L) of C_2D_4 at 150 K, followed by a 3 K/sec temperature ramp to 750 K while monitoring both expected products and possible adventitious species (CO, H_2O). 150 K

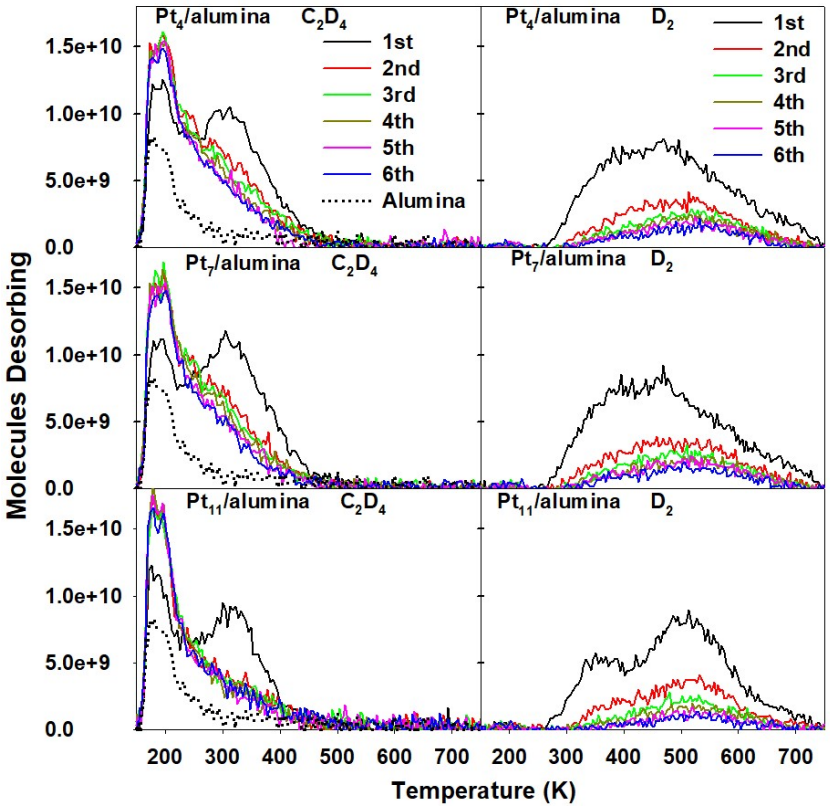

Figure 1. C_2D_4 and D_2 desorption, from Pt_n/alumina (n = 4, 7, 11)

was chosen for dosing to minimize C_2D_4 adsorption on the alumina support. The only significant desorption signals for Pt_n/alumina were for intact C_2D_4 and for D_2, and runs to higher final temperature showed that desorption was complete by 750 K. The D_2 signal has been corrected for the small mass 4 contribution from dissociative ionization of C_2D_4.

The dotted curves show the desorption observed in the 1st TPD run for a Pt-free alumina sample. No D_2 was observed, and the calibrated intensity (see "Methods") of the weak C_2D_4 desorption near 200 K was ~2 x 10^{13} C_2D_4/cm^2, or just over 1% of a C_2D_4 monolayer. Thus, the alumina support had a small density of sites capable of binding ethylene at 150 K, but these molecules simply desorbed intact below 250 K. No change was observed in repeated TPD runs.

For all Pt_n/alumina samples, both C_2D_4 and D_2 desorption were observed, with size-dependent

variations in the intensities and sub-structure of the desorption features. C_2D_4 desorption was bi-modal, with a ~200 K peak similar to that for Pt-free alumina but with higher intensity, and a stronger feature only seen with Pt_n present, beginning near 230 K and going to completion by ~450 K. In the 2nd and subsequent TPD runs, the ~200 K peak strengthened, while the higher temperature feature weakened rapidly.

D_2 desorption was observed between ~270 K and ~750 K for all Pt_n, with intensity that decreased rapidly over the series of TPD runs, and generally shifted toward higher temperatures. D_2 desorption was clearly bimodal for Pt_{11}, with an initial feature that peaked near 360 K, followed by a stronger feature starting near 400 K and peaking at ~520 K. For Pt_4 and Pt_7, the bimodal structure was less obvious, possibly because the higher temperature feature shifted ~50 K to lower temperature, overlapping to varying degrees with the low temperature feature. The bimodal structure generally became less pronounced in subsequent TPD runs.

A calibration method outlined previously[18] was used to convert the measured $C_2D_4^+$ and D_2^+ ion signals to numbers of desorbing C_2D_4 and D_2 molecules, and the results are summarized in Tables S1 through S3, reported in terms of numbers of molecules *per* deposited cluster. The Pt_n/alumina values were corrected by subtracting the desorption observed from Pt-free alumina, i.e., the tabulated values represent desorption from Pt_n-associated sites. Both the total Pt-associated C_2D_4 desorption, and the T >260 K desorption ("High T C_2D_4") values are reported. The tables also report two derived values. "Adsorbed C_2D_4/cluster" is the number of C_2D_4 molecules that adsorbed into strong ($T_{desorption}$ >260 K) Pt-associated binding sites during the 150 K C_2D_4 dose preceding each TPD heat ramp, calculated by assuming that all adsorbed C_2D_4 either desorbed intact or decomposed to liberate 2 D_2 molecules. "Accumulated C atoms/cluster", is simply the amount of carbon that accumulated on the samples,

calculated assuming each desorbing D_2 molecule left behind one C atom. This assumption was previously tested by post-TPD C 1s XPS.[16] We estimate ~10% relative uncertainty in comparing C_2D_4 vs. D_2 desorption or comparing desorption in different experiments, but ~50% uncertainty in the absolute values. Non-integer molecules/cluster values may simply reflect this absolute uncertainty, however, multiple cluster isomers were likely to have contributed to the desorption, each with its own C_2D_4 adsorption/decomposition properties. Note that the "alumina" values given in each table are simply the ~2 x 10^{13} C_2D_4/cm^2 that desorbed from Pt-free alumina, normalized to the density of deposited clusters in each Pt_n/alumina sample.

Roughly speaking, during the 150 K saturation dose prior to the first TPD runs on the Pt_n/alumina samples, ~n/2 C_2D_4 molecules/cluster adsorbed into strong Pt-associated sites, in addition to a smaller amount in weakly bound sites, mostly associated with the alumina support. Roughly half this strongly bound C_2D_4 desorbed intact below 400 K, while the balance decomposed producing D_2 between ~270 and ~700 K, leaving ~n/2 carbon atoms behind on the surface.

As noted above, ethylene TPD studies on bulk Pt surfaces found that intact ethylene desorption dominated at high coverages, but for coverages below ~0.5 ML, decomposition leading to H_2 desorption dominated,[26] with the change in branching attributed to decomposition requiring empty sites to bind the decomposition products. For our clusters, the branching between intact dissociation and decomposition generating D_2 also appears to follow this pattern, i.e., the initial desorption from C_2D_4-saturated clusters was entirely of intact C_2D_4, with D_2 observed only at higher temperatures after significant C_2D_4 desorption had occurred.

In the second TPD runs, the numbers of C_2D_4 molecules adsorbed into strong binding sites during the initial 150 K dose dropped by roughly half, and continued to drop more slowly in subsequent runs,

reaching values ≤30% of the 1st run values in the 6th TPD run. Both the >260 K intact C_2D_4 desorption and D_2 desorption decreased, the latter by factors of ~84% for Pt_4 and Pt_7, and by ~90% for Pt_{11} over the six TPD runs. Thus, we conclude that the combination of carbon deposition and sintering reduced the numbers of strong C_2D_4 binding sites available. This decrease was only partially offset by increases in the numbers of weak-binding sites, from which C_2D_4 simply desorbed intact below 260 K. The increase in <260 K desorption is attributed C_2D_4 bound at weak Pt-associated binding sites, rather than at alumina sites, because no such increase was observed in repeated TPD runs on Pt-free alumina.

The obvious question is whether these changes resulted from carbon deposition, from thermal effects such as cluster isomerization or sintering, or from both. Purely thermal effects were probed by experiments such as that presented in Fig. S1 and Table S4, in which a set of six TPD heat ramps were performed for a Pt_4/alumina sample, but with no C_2D_4 dose prior to the 1st heat ramp. Thus, at the start of the 2nd TPD run in this experiment, the sample had been heated to 750 K, but without carbon deposition. The amounts of D_2 and high T C_2D_4 desorption observed when the once-heated sample was given a C_2D_4 TPD run were 45% and 17% lower, respectively, compared to the amounts during the 1st TPD run on as-deposited Pt_4/alumina, but substantially larger decreases (60% and 30%, respectively) were observed following a single C_2D_4 TPD run on as-deposited Pt_4/alumina. Thus, both carbon deposition and thermal isomerization/sintering contribute to the loss of strong Pt-associated C_2D_4 binding sites and the resulting reduction in decomposition to produce D_2.

2. The effects of Ge addition to Pt_n/alumina

Fig. 2 shows TPD data for Pt_4Ge/alumina, Pt_7Ge_2/alumina, and $Pt_{11}Ge_4$/alumina measured using the same protocol used for Pt_n/alumina (Fig. 1). Both C_2D_4 and D_2 were observed to desorb, but the relative intensities and run-to-run stabilities were very different from the Pt_n results. Tables S5-S7 give

the numbers of molecules that desorbed, the inferred numbers of C_2D_4 molecules adsorbed into strong ($T_{desorption}$ > 260 K) binding sites prior to each TPD run, and the cumulative carbon deposition. For comparison, the C_2D_4 desorption from a Ge-treated alumina substrate ("Ge/alumina") is also shown. No D_2 desorption was observed from that sample.

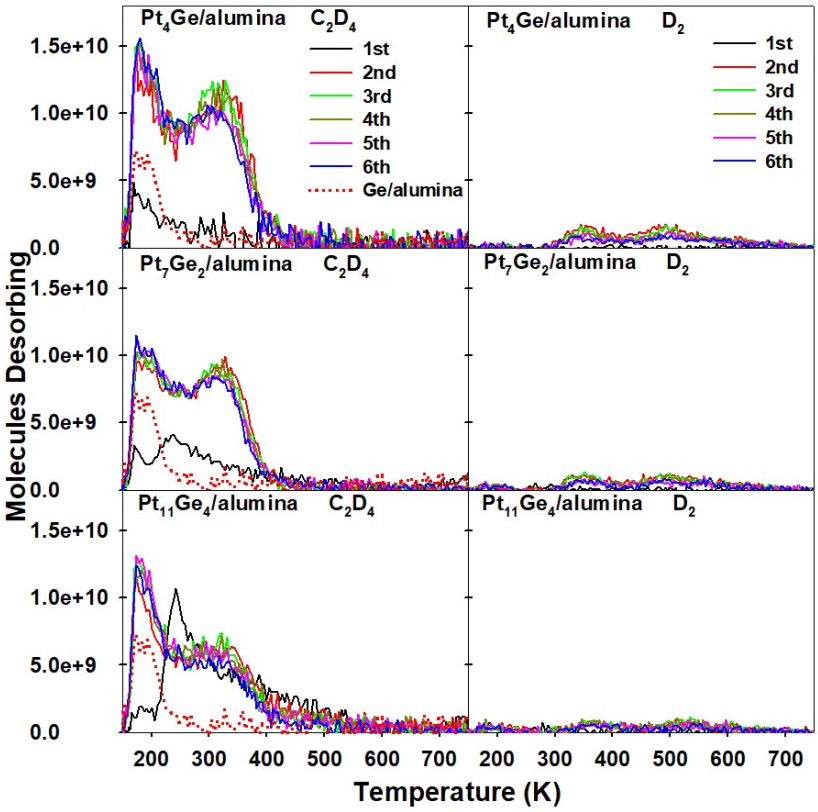

Figure 2. C_2D_4 and D_2 desorption from Pt_nGe_m/alumina (n = 4, 7, 11) model catalysts with the indicated stoichiometries.

Note that the 1st TPD run for the Pt_nGe_m samples was different from the 2nd-6th runs. As noted, the final step in the Ge-treatment process was to ramp the sample temperature to 750 K to desorb H and residual Cl as HCl and H_2. For the experiments in Fig. 2 the samples were dosed with C_2D_4 at 150 K prior to this heat ramp, thus the 1st C_2D_4 TPD run was also the final step of the Ge treatment. Because H and Cl were present when the C_2D_4 was dosed, less C_2D_4 adsorbed, and the desorption products also changed, as shown in Fig. S2 for Pt_7Ge_2/alumina. No D_2 was observed, and in addition to small signals for HCl and C_2D_4 desorption, signal for $C_2D_4H_2^+$ was observed, resulting from reaction between adsorbed C_2D_4 and H. The important point is that after this first heat ramp, only C_2D_4 and D_2 were

observed in subsequent C_2D_4 TPD runs, and the intensities were essentially identical if the 1st heat ramp was done without the 150 K C_2D_4 dose (Table S8). Thus, the first heating, with or without C_2D_4 present, generated clean Pt_nGe_m/alumina samples that were then probed in the 2nd – 6th C_2D_4 TPD runs. This numbering scheme was used to keep the thermal history of the Pt_nGe_m/alumina and Pt_n/alumina samples consistent, but analysis of the Pt_nGe_m/alumna TPD data is focused on runs 2 – 6. Note that for Ge/alumina the TPD results were identical in runs 2 – 6, and Fig. 2 shows the 2nd run signal.

Comparison of Figs. 1 and 2 (tables S1-S3 and S5-S7), shows that Ge addition to Pt_n had several effects. Ca. 30% less C_2D_4 desorbed from the Ge/alumina surface than from alumina, indicating that Ge blocked some sites for 150 K C_2D_4 adsorption on alumina, presumably because both Ge and C_2D_4 adsorption tended to occur at similar alumina defect sites. Intact C_2D_4 desorption occurred in distinct low and high temperature features for both Pt_n/alumina and Pt_nGe_m/alumina but run-to-run stability was far higher for the Ge-treated samples. D_2 desorption (i.e., carbon deposition) was largely, but not entirely suppressed in the Ge-treated samples and occurred with distinctly bimodal temperature dependence.

To facilitate comparisons between different size Pt_n and Pt_nGe_m samples, Fig. 3 plots the numbers of C_2D_4 molecules that adsorbed, desorbed, and decomposed during the TPD sequences for Pt_n/alumina and Pt_nGe_m/alumina, including the Pt_4/alumina sample that was flashed to 750 K prior to the TPD sequence. The results for a Pt_4Ge/alumina sample that was heated to 750 K twice prior to the first C_2D_4 TPD run (Table S8) are not plotted because they were essentially identical to those for Pt_4Ge from Fig. 2. The figure is plotted in terms of C_2D_4 molecules *per* Pt atom to facilitate comparisons between cluster sizes, and values are shown from the 1st, 2nd, and 5th TPD runs on the Pt_n samples, and from the 2nd, 3rd, and 6th runs for the Pt_nGe_m. The total bar heights represent the numbers of C_2D_4 molecules adsorbed

into strong binding sites ($T_{desorption}$ > 260 K) prior to each TPD run, the lower segments show the intact C_2D_4 desorption above 260 K, and the upper segments represent C_2D_4 molecules that decomposed resulting in desorption of two D_2 molecules. Comparing the 2nd run Pt_nGe_m/alumina data to the 1st run data for Pt_n shows that Ge addition (with 750 K heating to desorb H and Cl) substantially reduced the *per*-Pt number of C_2D_4 binding sites, but because of the stabilizing effects of Ge addition, the numbers of binding sites remaining at end of the TPD sequences were higher for Pt_nGe_m than for the Pt_n.

One interesting point is that by end of the 6-run sequence, the Pt_n/alumina samples had accumulated 4.3 C atoms/Pt_4, 7.7 C/Pt_7, and 9.7 C/Pt_{11} (Tables (S1-S3). Thus, for the Pt_n, the carbon accumulation increased almost linearly with cluster size, such that the final C atom/Pt atom ratios were all near unity. In contrast, the final (5 run) carbon accumulations were 1.2

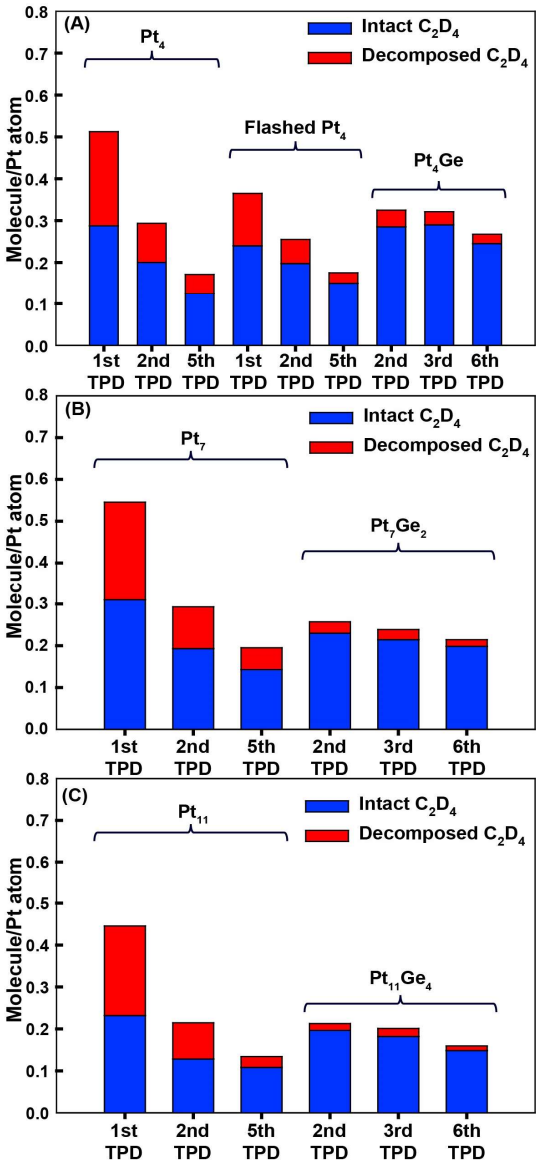

Fig. 3. Desorption *per* Pt atom in selected TPD runs for Pt_n/alumina and Pt_nGe_m/alumina for n = 4 (A), 7 (B), and 11 (C). Blue = intact >260K C_2D_4 desorption. Red = C_2D_4 that decomposed to 2 D_2 + 2C. Total bar height = total C_2D_4 adsorbed prior to each TPD run. Relative uncertainties for comparing values are ~10%, and absolute uncertainties are estimated to be ~50%.

C/Pt_4Ge, 1.4 C/Pt_7Ge_2, and 1.8 C/$Pt_{11}Ge_4$, i.e., the carbon accumulations *per* Pt_nGe_m cluster varied weakly with increasing cluster size, such that the C atom/Pt atom ratios decreased from ~0.35 for Pt_4Ge to just 0.16 for $Pt_{11}Ge_4$, implying that cluster size continued to be a controlling factor over the TPD sequence. Note that the fact that up to ~2 C atoms can accumulate *per* cluster with little effect on the TPD temperature dependence or intensity implies that carbon deposition has minimal effect on the strength and number of C_2D_4 binding sites on Pt_nGe_m.

Figs. 1 and 2 show diminishing amounts of D_2 desorption/carbon deposition over the TPD sequence, and in our previously reported C_2D_4 TPD study of Pt_4/alumina and Pt_4Ge/alumina,[16] we carried out 21-run TPD sequences to see if carbon deposition stopped at some level. The D_2 desorption signal continued to decrease over the 21 runs, eventually dropping below the small m/z=4 mass spectrometer background, implying that carbon deposition asymptotically approaches some limiting value. For the Pt_n clusters, this value exceeds one C atom/Pt atom, but for the Pt_nGe_m clusters, coking appears to self-limit at a relatively small value, of roughly two C atoms/*cluster*, approximately independent of cluster size.

3. The effects of alumina-bound Ge

As noted, the Ge treatment process resulted in significant numbers of alumina-bound Ge atoms in the Ge-treated samples, i.e., the Pt_nGe_m/alumina samples had Ge bound to the Pt clusters with additional Ge in nearby alumina sites. Ge-treated, Pt-free alumina was found to have ~5.9 x 10^{13} Ge/cm^2 (~4% of a Ge monolayer), and the alumina-bound Ge coverage on the Pt_nGe_m/alumina samples would have been ~90 % of this value because the Pt_n clusters would have occupied ~10% of the alumina surface. The effects of this alumina-bound Ge on C_2D_4 TPD were tested by the experiments shown in Fig. S3, where alumina supports were pre-treated with Ge and heated to 750 K (to desorb HCl) prior to Pt_n deposition

and probing by six C_2D_4 TPD runs. The conclusion from comparing Figs. 1, 2, and S3 is that the alumina-bound Ge present on the Pt_nGe_m/alumina samples would have had minimal effect on the chemistry of the Pt_nGe_m clusters. The results also indicate that diffusion of as-deposited Pt_n on the Ge/alumina surface is not facile, but that diffusion may occur when the samples are heated repeatedly.

4. The effects of Ge and carbon addition on hydrogen desorption from Pt_n

One question is whether D_2 desorption during C_2D_4 TPD is rate-limited by C_2D_4 decomposition or by the kinetics for recombinative desorption of the resulting D atoms. We probed this issue by measuring (Fig. 4) the D_2 desorption observed following 150 K saturation D_2 doses followed by heating at 3 K/sec. Data are shown for as-prepared Pt_4 and Pt_4Ge samples, and for Pt_4 and Pt_4Ge samples given two C_2D_4 TPD runs prior to the D_2 TPD run. For comparison, the figure also reproduces the D_2 signal observed during the 1st C_2D_4 TPD experiment on Pt_4/alumina (Fig. 1). A small HD signal was observed for the as-deposited Pt_4 sample, attributed to adventitious H_2 adsorption during deposition, and the "D_2" signal for that sample is the sum of the HD and D_2 signals.

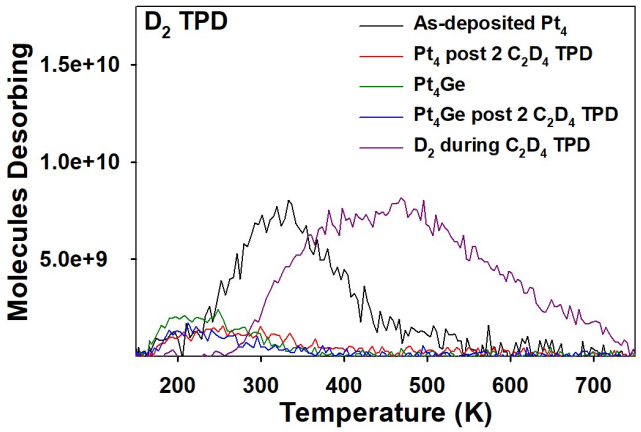

Fig. 4. Recombinative D_2 desorption following 150 K D_2 exposures to Pt_4/alumina and Pt_4Ge/alumina, as-prepared and after two C_2D_4 TPD runs. Also shown is the D_2 desorption observed in the first C_2D_4 TPD run on Pt_4/alumina.

For D_2-dosed Pt_4/alumina, desorption started near 200 K, peaked near 330 K, and was complete by ~450 K, similar to hydrogen recombinative desorption reported for both Pt clusters and bulk Pt

surfaces.[20, 58, 59] Desorption of D_2 during C_2D_4 TPD began near 300 K, peaked near 470 K, and continued to 750 K, with integrated intensity roughly double that observed during D_2 TPD. The higher D_2 onset temperature during C_2D_4 TPD supports the conclusion that D_2 desorption is rate-limited by the C_2D_4 decomposition step, rather than D-D recombinative desorption.

It is conceivable that the high D_2 desorption onset temperature during C_2D_4 TPD partly results from strengthening of Pt-D binding due to the presence of carbonaceous co-adsorbates on the clusters, and this possibility was tested by subjecting a Pt_4/alumina sample to two C_2D_4 TPD runs prior to the D_2 TPD experiment, depositing ~4 C atoms/Pt_4. As shown by the "Pt_4 post 2 C_2D_4 TPD" data, both the D_2 signal intensity and desorption temperatures decreased substantially, implying that co-adsorbed carbon actually weakened Pt-D binding, and also reduced the number of sites capable of supporting 150 K D_2 adsorption.

As-prepared Pt_4Ge/alumina also gave weak D_2 TPD signal, peaking near ~200 K, implying that a single Ge atom also substantially decreased the D_2 chemisorption probability and reduced the Pt-D binding strength. The onset of D_2 desorption was well below the D_2 desorption onset for C_2D_4 TPD from Pt_4Ge, again suggesting that C_2D_4 decomposition is rate limiting. Subjecting Pt_4Ge to two C_2D_4 TPD runs prior to the D_2 TPD run resulted in only a small additional reduction in the D_2 desorption signal, with no significant effect on the temperature dependence.

B. CO TPD as a probe of accessible Pt sites

Figs. 1 and 3 show that repeated C_2D_4 TPD runs on Pt_n/alumina decreased the numbers of strong ($T_{desorption}$>260 K) Pt-associated C_2D_4 binding sites and the fraction of adsorbed C_2D_4 that decomposed, but also increased the number of weak C_2D_4 binding sites. Ge addition reduced the initial number of strong C_2D_4 binding sites; however, it also stabilized these sites against the effects of carbon deposition

and sintering. One obvious question is whether the effects of carbon or Ge addition are geometric, due to site blocking by C or Ge atoms, or if the main effects are electronic, changing the nature and strength of C_2D_4-cluster binding. For Pt_nGe_m/alumina, another question is whether the high stability simply results from reduced carbon deposition or if Ge also suppress sintering, as seems to be implied by the TPD results.

Because CO binds strongly to Pt, CO TPD was used to probe changes in the numbers and strengths of accessible Pt sites under different conditions. Six sequential CO TPD runs were used to probe as-prepared Pt_n/alumina and Pt_nGe_m/alumina samples, with ^{13}CO dosed at 150K prior to each 3 K/sec heat ramp, and both ^{12}CO and ^{13}CO desorption monitored. Fig. 5 shows the results for alumina, Pt_4, Pt_7, Pt_{11}, Ge/alumina, Pt_4Ge, Pt_7Ge_2, and $P_{11}Ge_4$ samples, and Tables S9-S11 summarize the molecular bookkeeping, using the same calibration approach used for the C_2D_4 TPD, with estimated ~10% relative and ~50% absolute uncertainties. Values are given for "Total CO/cluster" and for "High T CO", defined as $T_{desorption} > 335$ K for Pt_n and 300 K for Pt_nGe_m, reflecting the onset of the main high T desorption feature. Significant ^{12}CO signal was observed only for the 1st TPD run for Pt_4/alumina due to background CO adsorbed during cluster deposition, and for that run, the sum of $^{12}CO + {}^{13}CO$ signals is plotted.

Roughly 2 x 10^{13} molecules/cm^2 (~0.01 ML) desorbed from Pt-free alumina below 250 K, attributed to binding at alumina defects. CO desorption from Ge/alumina was ~15% weaker but extended to slightly higher temperatures, suggesting that the ~0.04 ML of alumina-bound Ge blocked 150 K adsorption at some alumina defect sites, but also slightly increased the strength of CO binding at some Ge/alumina sites. To facilitate comparison to the cluster-containing samples, the numbers of CO that desorbed from alumina and Ge/alumina samples are tabulated in terms of "molecules/cluster", i.e.,

the desorption/cm^2 divided by the cluster coverages for each cluster size.

The Pt_n/alumina samples also had weak desorption below 200 K attributed to the alumina support, but the main desorption occurred in a broad feature between 400 and 600 K, along with weaker, structureless desorption in the 200 to 400 K range. Over the TPD sequence, the high T desorption feature weakened and shifted to lower temperatures, increasing the desorption between 200 and 400 K for Pt_4 and Pt_7, but not for Pt_{11}. The total 1st run CO desorption (corrected for alumina-bound CO) ranged from 3.73 CO/Pt_4, to 6.22 CO/Pt_7,to 6.76 CO/Pt_{11}, i.e., the CO:Pt ratio was nearly unity for Pt_4 and Pt_7 but only ~0.6 for Pt_{11}, indicating that all Pt atoms in Pt_4 and Pt_7 were accessible in agreement with DFT studies (see below), while Pt_{11} retained 3D structure with some Pt atoms buried, even when saturated with CO. Both the total CO/cluster and high T CO/cluster decreased gradually over the 6 TPD runs, with the largest decrease for Pt_{11}. Given that these changes must have resulted from processes like cluster isomerization or sintering, the implication is that Pt_{11} is less thermally stable than Pt_4 and

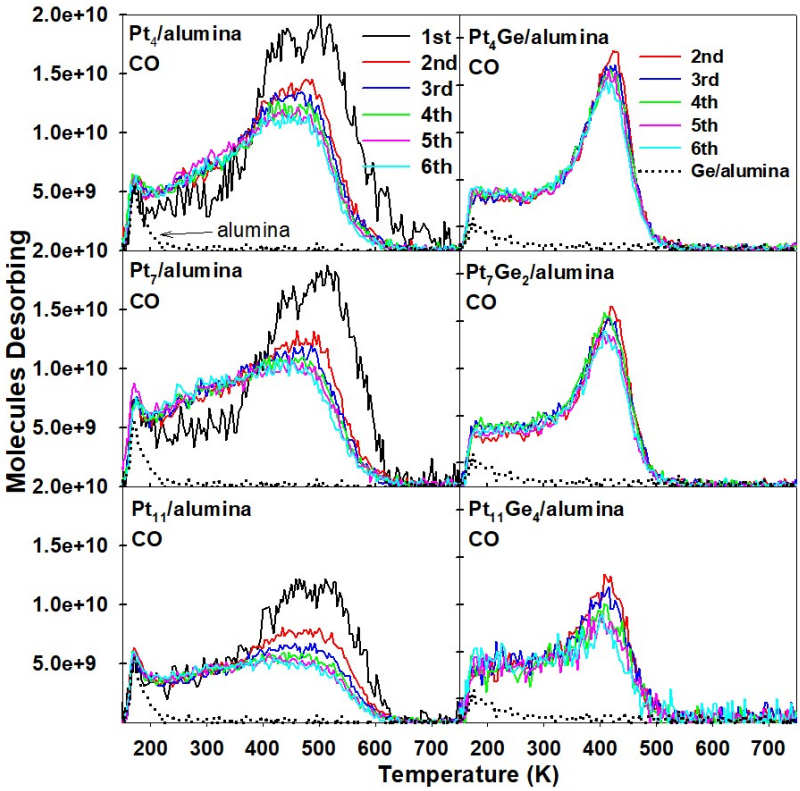

Fig. 5. CO desorption from Pt_4, Pt_7, Pt_{11}, Pt_4Ge, Pt_7Ge_2 and $Pt_{11}Ge_4$ on alumina.

Pt_7, consistent with previous results showing that Pt_4 and Pt_7 are relatively stable with respect to other sizes in the Pt_1 to Pt_7 size range.[15]

Prior to the CO TPD sequence, the Pt-$_n$Ge$_m$/alumina samples were flashed to 750 K to remove H and Cl from the Ge-addition process, then CO TPD was done as the 2nd – 6th heat ramps, labeled in this way to keep the thermal history of all the samples consistent. Compared to the Pt_n the initial numbers of CO molecules desorbing *per* cluster were lower for the Pt_nGe_m (by ~48% for n=4, 7, ~30% for 11), but both the molecules/cluster and the temperature dependence of the desorption were far more stable in repeated TPD cycles. All five TPD runs had relatively sharp peaks between ~375 and 475 K, along with weaker, featureless desorption at lower temperatures. Thus, the CO TPD results imply that Ge addition reduced the initial numbers of CO binding sites, but stabilized the clusters against sintering or other thermal changes that would have reduced the number or strength of the CO binding sites.

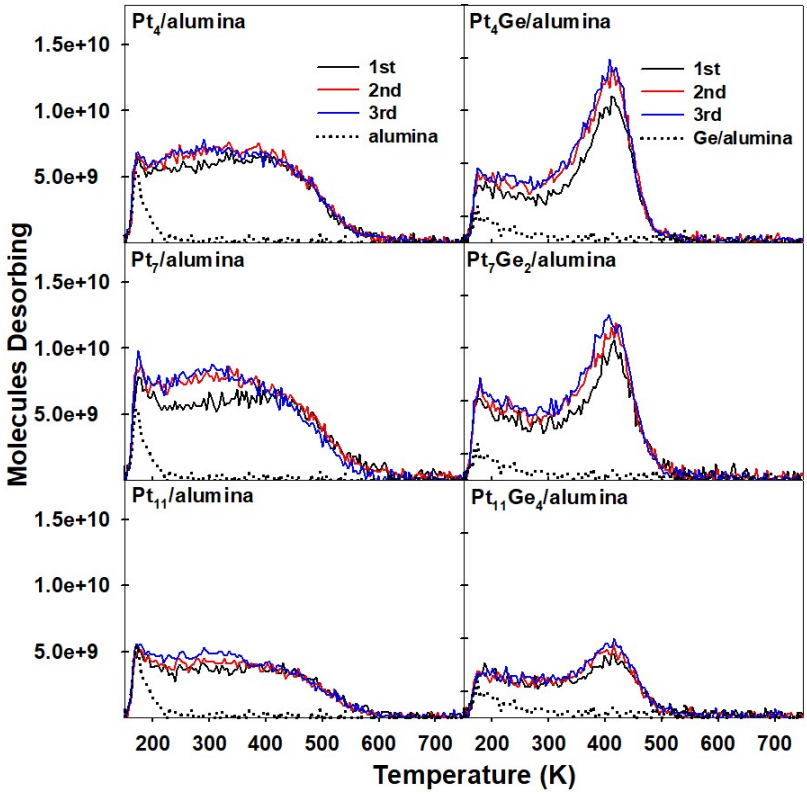

Fig. 6. CO desorption from Pt_4, Pt_7, Pt_{11}, Pt_4Ge, Pt_7Ge_2 and $Pt_{11}Ge_4$ clusters on alumina, after three prior C_2D_4 TPD runs.

To examine the effects of carbon deposition on CO binding, separate sets of Pt_n and Pt_nGe_m samples

were first given three C_2D_4 TPD runs, then probed by three CO TPD runs, shown in Fig. 6 and Tables S12-S14. Note that the CO desorption intensities *increased* slightly from run to run – an artifact of slowly decreasing C_2D_4 background pressure following the three C_2D_4 TPD runs. As a result, there was competition for Pt adsorption sites between background C_2D_4 and CO, especially during the first CO TPD run, therefore we use the final CO TPD run data for each sample when comparing numbers of CO binding sites.

For the Pt_n samples, comparing the same numbered TPD runs in Figs. 5 and 6 shows the combined effects of thermal sintering/isomerization and carbon deposition during the three C_2D_4 TPD runs, which would have deposited ~0.7 to 0.8 C atom/Pt atom on average. Compared to CO TPD without prior C_2D_4 TPD (Fig. 5), the most obvious effects were substantial weakening of the desorption between 400 and 600 K, with increased run-to-run stability of the CO desorption. Comparison to runs 4-6 in Fig. 5, where the samples were heated three times but without carbon deposition, implies that stabilization is an effect of carbon addition to the clusters. Taken together, the data for the Pt_n samples in Figs. 5 and 6 show that much of the initial loss of CO binding sites for Pt_n/alumina is attributable to thermal sintering/isomerization, with carbon deposition resulting in ~20% additional site loss, but also stabilizing the clusters against further thermal changes.

Comparison of Figs. 5 and 6 shows that three prior C_2D_4 TPD runs only decreased the number of strong CO binding sites by 16% for Pt_4Ge and by 12% for Pt_7Ge_2. Three C_2D_4 TPD runs would have deposited an average of 0.57 C atom/Pt_4Ge cluster, and 0.72 C/Pt_7Ge_2 cluster (0.14 and 0.10 C/Pt atom), but because C_2D_4 either desorbs intact or decomposes depositing two C atoms, we interpret this to mean that roughly a third of the clusters had accumulated two C atoms, with the rest remaining carbon free. Therefore, the fact that only 12 - 16% loss of CO binding sites occurred implies these very small Pt_nGe_m

clusters can accommodate two C atoms with only modest effects on the number or strength of the CO binding sites. The DFT results below show that CO binds only to Pt atoms, and not to Ge or C in the coked clusters. Curiously, the CO binding site loss caused by three prior C_2D_4 TPD runs was much larger for $Pt_{11}Ge_4$ (~56%), even though the amount of carbon that would have accumulated (~0.79 C/cluster) was only slightly higher than for Pt_7Ge_2 (0.72 C/cluster), and the C/Pt atom ratio (~0.07) was substantially smaller than those for Pt_4GeC_2 or $Pt_7Ge_2C_2$. Finally, note that despite the substantial variations in the intensities of the different desorption features, the desorption temperatures are quite similar for all three sizes of Pt_n and Pt_nGe_m clusters, with and without prior C_2D_4 TPD runs. Thus, while cluster size affects the numbers of different types of CO binding sites, the desorption energies for the various binding sites are nearly identical for all three cluster sizes.

C. He^+ Ion Scattering (ISS) Probes of Cluster and Adsorbate Morphology

ISS provides a complementary probe of the surface accessibility of Pt (and Ge) atoms, with the added benefit that it can show how Pt accessibility changes *during* a TPD run, using temperature-programmed ISS (TD-ISS).[60] Examples of raw ISS data are shown in Fig. S4 for Pt_7/alumina and Pt_7Ge_2/alumina samples probed as prepared, after a single 750 K heat ramp, and after one or six C_2D_4 TPD runs. Separate samples were used for each measurement to avoid damage effects. Experiments examining changes in the Pt and Ge ISS intensities as the He^+ beam slowly sputters the surface are presented in Fig. S5 and the associated discussion.

ISS peaks largely result from He^+ scattering from single atoms in the surface layer, giving well-defined scattered energies that identify the surface atom masses.[61] Sub-surface or multiple scattering events contribute mostly to a featureless background that is weak because He^+ is less likely to survive such events. Because all samples here had identical numbers of Pt atoms deposited, variations in the Pt

(and Ge) ISS intensities provide insights into changes in the fraction of Pt atoms present in the surface layer. For example, adsorbate-free Pt_n with single layer structures where all Pt atoms are in the surface layer should have the highest Pt intensities, while multi-layer/3D clusters should have lower intensities. The intensities for adsorbate-covered clusters are small because adsorbates block or shadow scattering from underlying Pt atoms, whereas adsorbates bound within or under the cluster surface layer do not attenuate the Pt ISS signal.[60]

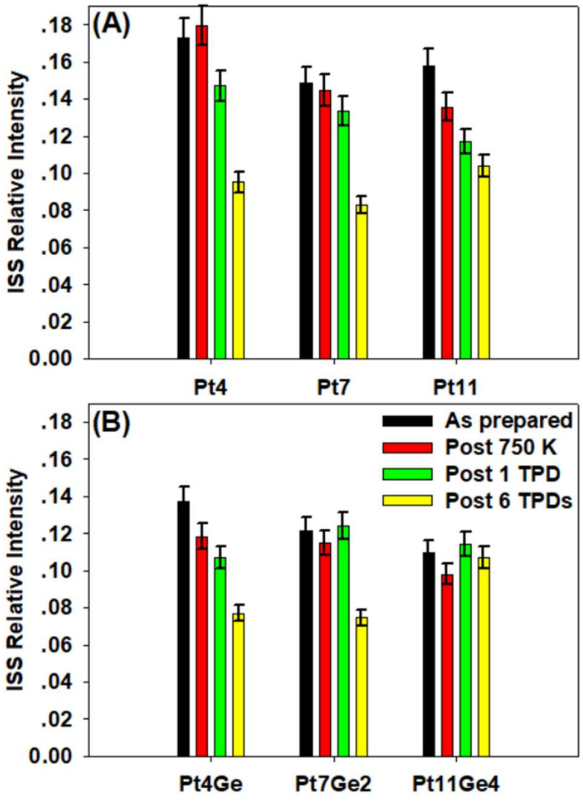

Fig. 7. Initial Pt exposure in ISS spectra of as prepared, post 750 K heat, post 1 TPD and post 6 TPDs of (A) Pt and (B) Pt_nGe_m clusters.

1. Effects of sample treatment of ISS intensities

Fig. 7 summarizes the results from Fig. S5, giving Pt intensities for Pt_n and Pt_nGe_m samples under different conditions. The error bars reflect uncertainties from both statistical noise and from small day-to-day variations in the He^+ beam properties and other experimental conditions, as estimated from the reproducibility observed in experiments on identically prepared samples. For the as-prepared Pt_n samples, where a small amount of adventitious CO adsorbed during cluster deposition, "adsorbate-free" intensities have been estimated by extrapolating the data in Fig. S5 to the limit of zero He^+ exposure.[62]

Relative to the estimated as-prepared values, 750 K heating (desorbing the CO) had little effect on the Pt ISS intensities for Pt_4 and Pt_7 and caused a ~10% reduction for Pt_{11}. The Pt intensities decreased after C_2D_4 TPD, by ~45% for Pt_4 and Pt_7, and by ~35% for Pt_{11} after 6 C_2D_4 TPD runs. While those attenuations are substantial, even larger attenuations would be expected if the ~1.5 C atoms/Pt atom deposited by six TPD runs were bound on top of the clusters.[60] Furthermore, if carbon were bound primarily on top of Pt, the post-TPD Pt intensities in Fig. S5 would have increased with He^+ exposure as overlying carbon sputtered away, contrary to observation.

The as-prepared Pt_nGe_m samples had Pt ISS intensities that were lower than those for the Pt_n, by ~10%, 18% and 32% for Pt_4Ge, Pt_7Ge_2, and $Pt_{11}Ge_4$, but the Pt ISS signals for the Pt_nGe_m were more stable after repeated C_2D_4 TPD runs, particularly for $Pt_{11}Ge_4$, where the Pt ISS intensity was essentially unaffected by C_2D_4 TPD. Thus, the effects of Ge addition on Pt ISS intensities generally follow the trends in numbers of strong CO or C_2D_4 binding sites observed in the TPD experiments, i.e., the numbers are decreased by Ge addition, but are far more stable in repeated TPD runs.

2. Temperature-dependent ion scattering (TD-ISS)

ISS can also be used to probe changes in cluster/adsorbate morphology during TPD, using the temperature-dependent ISS (TD-ISS) approach shown in Fig. 8. In essence, TD-ISS involves measuring ISS intensities after dosing a sample with reactants, and then at regular intervals as the sample is heated to drive desorption, sintering, and other processes that also occur during TPD.[60]

Fig. 8a shows TD-ISS probing C_2D_4 adsorption/desorption on Pt_4/alumina. Pt ISS intensities are plotted vs. temperature as black points connected by lines, referenced to the right-hand axis. C_2D_4 and D_2 desorption intensities observed during the 1st TPD run on Pt_4/alumina (Fig. 1) are shown as blue and red lines, referenced to the left axis. Pt ISS intensities measured for separate samples of as-deposited

Pt_4/alumina (~0.175) and Pt_4/alumina after a single C_2D_4 TPD run (~0.145) are indicated on the right-hand axis by a blue diamond and a red triangle, respectively.

The Pt ISS intensity after the 150 K C_2D_4 dose (0.04) was ~77% smaller than the value for as-deposited Pt_4/alumina, showing that C_2D_4 was bound on top of the clusters, attenuating scattering from Pt. Unsurprisingly, the Pt intensity remained constant as the sample was heated to 250 K, desorbing C_2D_4 from sites on the alumina support. The absence of intensity recovery between 250 and 400 K is more interesting, because most of the intact C_2D_4 desorption from Pt sites would have occurred in that temperature range. This finding is consistent with the proposal that as C_2D_4 desorption creates empty Pt sites, the remaining C_2D_4 decomposes, and

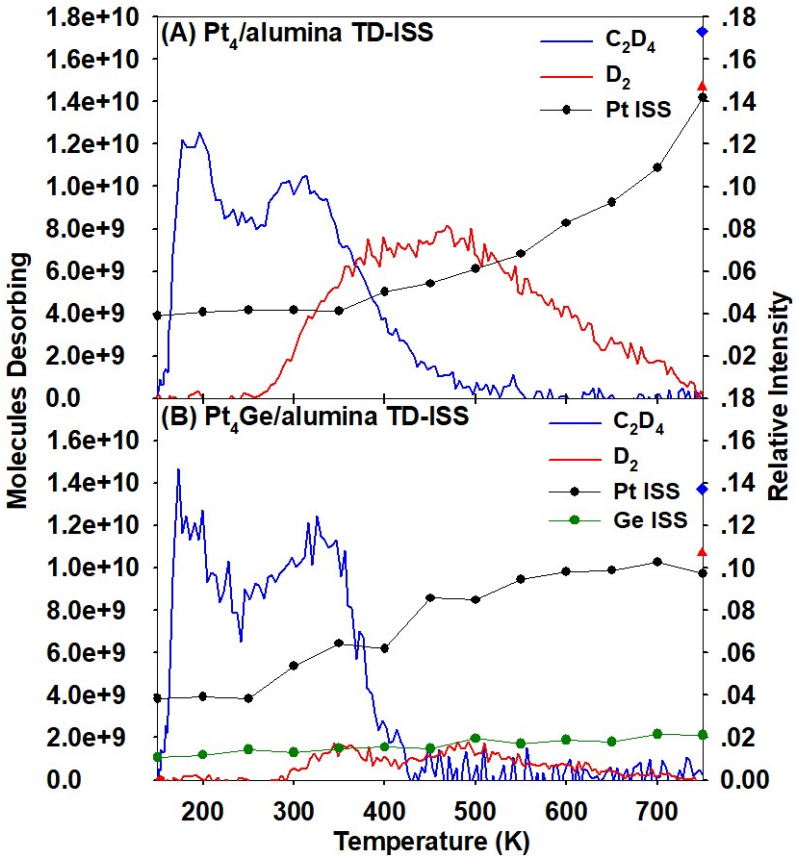

Fig. 8. Temperature-dependent ISS of Pt_4/alumina and Pt_4Ge/alumina samples with Pt (black) and Ge (green) ISS signals shown as solid points connected by lines. C_2D_4 and D_2 desorption intensities observed in C_2D_4 TPD on Pt_4 TPD and Pt_4Ge. Red dots on the right-hand axis show the Pt ISS intensities of similar samples measured after one C_2D_4 TPD run.

clearly the D and C_xD_y fragments occupy these Pt sites so that He^+ scattering from Pt remains strongly attenuated.

The Pt signal recovered significantly between 400 and 650 K, i.e., over the temperature range where D_2 desorption occurs, however, even at 650 K the Pt signal was still only ~55% of that for adsorbate-free Pt_4/alumina, even though desorption was essentially complete. Conversely, significant Pt signal recovery occurred between 650 and 750 K, even though little additional desorption would have occurred. Because only carbon would have been left on the surface at 650 K, the 55% Pt attenuation implies that the carbon atoms were initially bound in sites on top of the clusters, and the recovery of Pt signal above 650 K implies that these carbon atoms migrated to sites where they caused little attenuation of Pt ISS signal. Such sites could include carbon bound within or beneath the cluster surface layer, or bound to the alumina support.

Note that the final 750 K Pt intensity was nearly identical to the value measured after a normal TPD run on a separate sample, indicating that the He^+ exposure during TD-ISS had minimal effect on the final state of the Pt clusters. This final Pt intensity was 82% of the as-deposited value, i.e., some combination of carbon deposition and sintering during TPD caused a small decrease in the fraction of Pt in the surface layer, but clearly the clusters did not sinter into large 3D particles, which would have had resulted in much larger attenuations.[63]

The TD-ISS results for Pt_4Ge/alumina were quite different (Fig. 8b). After the 150 K C_2D_4 dose, the Pt ISS signal was ~28% of the as-prepared value, and the Ge intensity was ~60% of the as-prepared Ge value (~0.04), consistent with the DFT finding that C_2D_4 binds preferentially to Pt.[16] As in the Pt_4/alumina experiment, there was little change in Pt or Ge ISS signals as the temperature was stepped to 250 K, desorbing the support-bound C_2D_4, however, both Pt and Ge signals recovered significantly

between 250 and 400 K, spanning the higher temperature C_2D_4 desorption feature and the lower temperature D_2 desorption feature. Additional recovery of both Pt and Ge signals occurred as the temperature was stepped from 400 to 650 K, completing the D_2 desorption, but unlike Pt_4, there was little additional change above 650 K. These differences reflect the fact that a much larger fraction of C_2D_4 adsorbed on Pt_4Ge would have desorbed intact, with fewer decomposition products present at intermediate temperatures, and less carbon deposited.

From the perspective of coking effects on these model catalysts, one of the main conclusions from the ISS studies is that that the substantial post-750K-heating and post-TPD reductions in the numbers of strong Pt-associated C_2D_4 binding sites for Pt_n/alumina, are not simply due to carbon sterically blocking Pt binding sites, as was previously noted for the case of Pt_4/alumina.[23] Nonetheless, carbon atoms clearly have large effects on both C_2D_4 binding sites and the thermal stability of the samples in repeated TPD runs (Figs. 1, 2, 5 and 6). Therefore, DFT was used to probe the effects of both Ge and carbon addition to small Pt_n/alumina.

D. Theoretical Studies

1. Cluster Ensembles from DFT

We previously reported detailed DFT studies examining Pt_n/alumina (n = 4, 7, 8), including ethylene binding strengths on the thermally accessible cluster isomers and the effects of ethylene binding on cluster structures.[13] For Pt_4Ge/alumina and Pt_4GeC_2/alumina we reported DFT for all thermally accessible isomers of the bare clusters, the binding of one or more ethylene molecules, and the activation energies for dehydrogenation reactions of adsorbed ethane, ethylene, and acetylene.[16, 23]

An excited cluster isomer was found to be responsible for the observed self-limiting coking of Pt_4Ge,[16] i.e., including the energetically accessible isomer ensemble was critical to understanding the chemistry of

the n=4 clusters. Unfortunately, the numbers of potential cluster isomers, of cluster-support binding

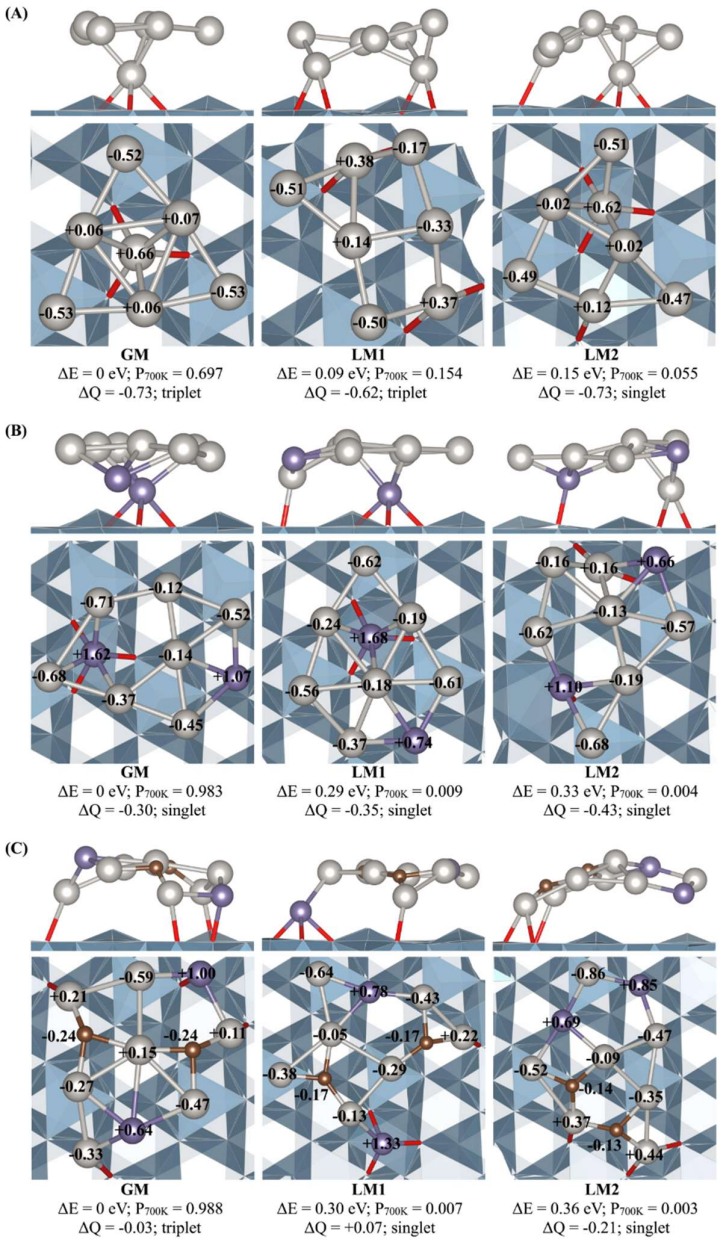

Fig.9. Top and side views of the global minimum (GM) and first two local minima (LM1, LM2) for (A) Pt_7, (B) Pt_7Ge_2, and (C) $Pt_7Ge_2C_2$. Energies (ΔE) are relative to the GM. The Boltzmann population at 700 K (P_{700K}), net support-to-cluster electron transfer (ΔQ), and spin state are shown. Bader charges are shown on each corresponding atom. Grey = Pt, purple = Ge, and brown = C.

geometries, and of possible C_2H_4 or CO adsorption geometries on the clusters all increase rapidly with cluster size, as does the cost per calculation, making such exhaustive studies infeasible for the larger Pt_n, Pt_nGe_m and $Pt_nGe_mC_n$ systems. We did a more limited C_2H_4 and CO binding study for the Pt_7-based systems, described below, including only the cluster global minimum (GM) and the two lowest energy local minimum isomers, LM1 and LM2. Even with this limitation, the computational cost was ~4 million CPU hours, and we estimate that the cost for a similar, limited computational study of the Pt_{11}-based systems would exceed 50 million CPU hours. Fortunately, many aspects of the experimental results are quite similar for all three cluster sizes studied, including the observation that coking self-limits at ~2 C atoms/Pt_nGe_m cluster for all sizes. The DFT results for the Pt_7- and Pt_4-based systems also show many similarities, thus, we feel that the insights from the Pt_4- and Pt_7-based calculations can reasonably be applied to understanding the Pt_{11}-based clusters as well.

We performed global optimization for Pt_7, Pt_7Ge_2, and $Pt_7Ge_2C_2$ on α-alumina and then based all other calculations on the structures for the global minimum (GM) and two low-lying local minima (LM1 and LM2) isomers. Their top and side views are shown in Fig. 9, along with the energies relative to the GM, the spin states, 700 K Boltzmann populations (P_{700K}), and the net charge on the clusters (ΔQ). The populations were calculated at 700 K to include isomers that would be populated during TPD cycling, where desorption is essentially complete at this temperature. For Pt_7, the GM adopts a prismatic structure, which comprises 70% of the 700 K Boltzmann population. About 20 isomers were found within 0.5 eV of the GM, thus, due to the strong fluxionality, several Pt_7 isomers are expected to be populated in the experimental temperature range. In contrast, only 6 and 5 isomers, respectively, were found within 0.5 eV of the GM for Pt_7Ge_2 and $Pt_7Ge_2C_2$, making them unusually non-fluxional for a Pt-based cluster of this size. Given the DFT energies, the GMs of both Pt_7Ge_2 and $Pt_7Ge_2C_2$ would

dominate the distribution (P_{700K} > 98%), with small LM1 and insignificant LM2 populations. Indeed, similarly low fluxionality was also noticed for Pt_4Ge and Pt_4GeC_2.[16] The isomers of Pt_7Ge_2 resemble the GM of Pt_7 with all the Pt atoms exposed, and the Ge atoms either within or beneath the surface layer. In general, Pt_7Ge_2 has one centrally located Ge atom that coordinates with 3 or 4 Pt atoms, with a second Ge atom near the cluster periphery, coordinated with 3 Pt atoms. No accessible isomers with direct Ge-Ge bonds were found. For $Pt_7Ge_2C_2$, the isomers are very similar to those of Pt_7 and Pt_7Ge_2, in which all the Pt are exposed, and the added C atoms sit on the edge of the clusters. The structures of $Pt_7Ge_2C_2$ are quasi-planar with features similar to the isomers of Pt_4GeC_2, i.e., the Ge atoms are bound in sites near the cluster periphery, coordinated to 2 to 4 Pt atoms, while the C atoms are more centrally located, each bonded to three Pt atoms. In contrast to Pt_4GeC_2, $Pt_7Ge_2C_2$ does not have direct C-C bonds for the accessible isomers. None of the $Pt_7Ge_2C_2$ (or Pt_4GeC_2) isomers have direct Ge-C bonding, and in all cases, the carbon atoms are in the plane of the cluster, rather than on top of Pt atoms. The latter point is consistent with the ISS experiments (Fig. 7), which showed that carbon tends to bind in sites where it does not strongly attenuate He^+ scattering from Pt.

The Pt_4Ge calculations found that both Ge and C additions strongly affected the charge distribution within the clusters.[16, 23] Additionally, the structural similarity among Pt_7, Pt_7Ge_2, and $Pt_7Ge_2C_2$ as shown in Fig. 9 suggests that both the reduction in strong C_2H_4 binding sites and the enhanced thermal stability resulting from the addition of Ge and C to Pt is mainly driven by electronic effects rather than steric blocking of Pt binding sites. Therefore, Bader atomic charges were calculated to assess the effects of the heteroatoms on the metal charges. The isomers of Pt_7 all have net negative charges due to electron transfer from the support to the cluster, and roughly half the Pt atoms have negative atomic charges. The GM and LM1 of Pt_7 are spin triplets, while LM2 is a spin singlet.

In Pt_7Ge_2, the Ge atoms are electron donors, such that the Pt atoms become more negatively charged than in Pt_7, but with less net negative charge on the clusters as a whole. Pt atoms that are directly bound to Ge are generally the most negatively charged. The accessible isomers of Pt_7Ge_2 are singlets, due to spin quenching via covalent Pt-Ge bonding. The inclusion of carbon in $Pt_7Ge_2C_2$ further reduces electron transfer from the support to the cluster, despite the charge distribution of Pt and Ge atoms remaining similar to that in Pt_7Ge_2. The C atoms of $Pt_7Ge_2C_2$ have negative atomic charges, which aligns with their relatively high electronegativity. The Pt atoms that are bound to C are generally more positively charged, and the rest of the Pt atoms are slightly less negative than those of Pt_7Ge_2. The GM of $Pt_7Ge_2C_2$ is a triplet, while the LM1 and LM2 are singlets. Since ethylene adsorption is associated with electron transfer from Pt to the carbon atoms of ethylene,[13] the similar Pt charge distributions in Pt_7Ge_2 and $Pt_7Ge_2C_2$ suggests that their ethylene binding energies should also be similar, consistent with the observation that C_2D_4 desorption changed only slightly over the TPD sequence for the Pt_nGe_m/alumina samples (Fig. 2).

In summary, the intra-cluster Ge-to-Pt electron donation in Pt_7Ge_2 largely replaces the alumina-to-Pt electron donation observed in Pt_7. In $Pt_7Ge_2C_2$, the electron density shifts toward the C atoms, through synergistic electronic interactions with the Ge. The bonding in both Pt_7Ge_2 and $Pt_7Ge_2C_2$ is substantially more ionic than in Pt_7, and we propose that this ionic nature helps stabilize the clusters against sintering/ripening by increasing the energy barriers for diffusion of the clusters on the ionic alumina surface and for dissociation of atoms onto the surface, as was previously suggested to rationalize the high stability of Pt_nSn_m clusters.[14]

As anticipated from the similarities in TPD, the charge distributions of $Pt_7Ge_2C_2$ and Pt_4GeC_2 are also comparable. For the GMs of both clusters, the average Pt charge is -0.17 e in $Pt_7Ge_2C_2$ vs. -0.13 e

in Pt_4GeC_2, the average Ge charge is +0.82 e in $Pt_7Ge_2C_2$ vs +0.85 e in Pt_4GeC_2, and the average C charge is -0.24 e in $Pt_7Ge_2C_2$ vs. -0.15 e in Pt_4GeC_2. The similarity in charge distributions between the higher energy isomers is similar to that for the GM. Therefore, it is unsurprising to see Ge induces self-limiting coking in clusters of both sizes (and for $Pt_{11}Ge_4$). Under the joint influence of C and Ge, the Pt becomes less negatively charged, which invites less further coking since carbon functions here as an oxidant. In fact, coking itself (without Ge) causes a similar electronic effect, slightly inhibiting further coking,[23] but the effect of carbon alone is apparently too weak to prevent additional coking in subsequent TPD runs. Ge puts more electrons onto the incorporated C atoms, and that enhances the coke-inhibiting electronic effect.

Fig. 9 shows that both Ge and C tend to embed into the Pt-Pt network, rather than staying on top, but this still affects the geometries of available Pt binding sites. To examine the effects of Ge and C addition on cluster structure more systematically, we optimized the structures of $Pt_nGe_mC_2$ (n = 4-7, m = 0-2), and the complete mapping of the Pt-Pt, C-C, and C-Pt distances for all the isomers found is summarized in Figs. S6 – S10. The C-C and C-Pt distances for bonded atoms have narrow distributions, whereas the Pt-Pt distances for bonded/nearest neighbour Pt atoms are distributed between ~2.5 and 3 Å, therefore 3 Å was used as the upper limit to define bonded Pt-Pt pairs. The numbers of Pt-Pt, C-C, and C-Pt bonds for each isomer are given in Fig. S11, and to summarize these results, Fig. 10 reports the numbers of C-C, C-Pt, and Pt-Pt bonds averaged over the isomer ensembles, weighed by each isomer's 700 K Boltzmann population. 700 K was chosen for this purpose as being the temperature where desorption was essentially complete in the TPD experiments, i.e., to include all isomers that would be populated during TPD cycling. No low energy isomers with Ge-C bonds were found.

One obvious result is that the population of structures with the two C atoms bonded together

decreases rapidly with increasing numbers of Pt atoms, becoming negligible for clusters with ≥ 6 Pt atoms, whereas increasing numbers of Ge atoms favours C-C bonding in clusters with 4 or 5 Pt atoms. The numbers of C-Pt bonds are less dependent on cluster size and stoichiometry, tending to increase with increasing number of Pt atoms, but decrease with increasing Ge content, approaching a limit of 6 to 7 C-Pt bonds for the larger clusters, for which C-C bonds were not observed. The average numbers of Pt-Pt bonds increase with the number of Pt atoms/cluster, as expected, but the Pt-Pt bond numbers also increase with added Ge atoms for the smallest clusters, reflecting the enhancement of C-C bonding and corresponding suppression of Pt-C bonding. For $Pt_6Ge_mC_2$ and $Pt_7Ge_mC_2$, where C-C bonding was not observed, Ge addition reduced Pt-Pt bonding. Another conclusion from this analysis is that the tendency for coking to self-limit at 2C/cluster for the Pt_nGe_m, regardless of size, is uncorrelated with the tendency of the $Pt_nGe_mC_2$ products to have C-C bonds.

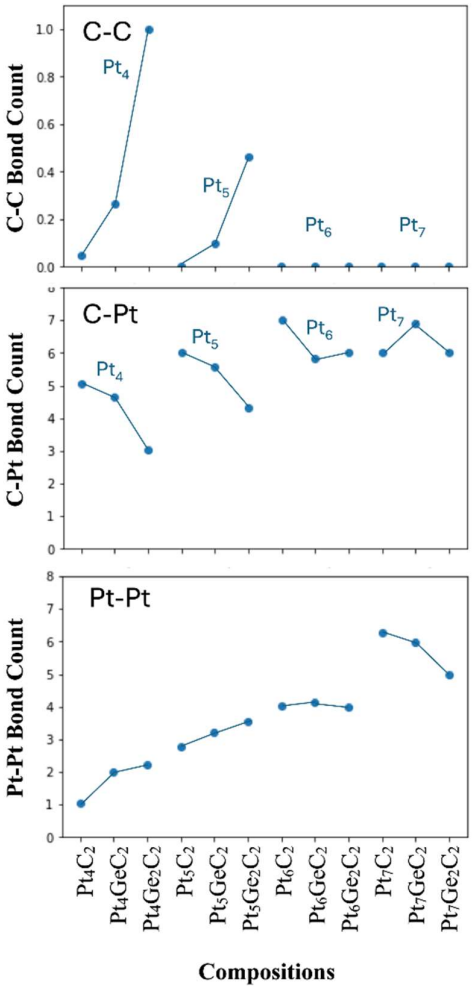

Fig. 10. Ensemble-averaged C-C, C-Pt, and Pt-Pt bond counts for $Pt_nGe_mC_2$ (n = 4-7, m = 0-2) from DFT global optimization. The thresholds used to define a bond were 1.75 Å for C-C, 2.25 Å for C-Pt, and 3.0 Å for Pt-Pt.

2. Ethylene Binding and Decomposition

To explore the enhanced coking stability of Pt-based catalysts doped with Ge (Figs. 1 and 2), we

used DFT to examine a single ethylene bound on Pt_7, Pt_7Ge_2, and $Pt_7Ge_2C_2$, including the GM, LM1 and LM2 isomers (Fig. 9). Unique binding modes (20 for Pt_7, 30 for Pt_7Ge_2, and 40 for $Pt_7Ge_2C_2$) were characterized for each isomer, and the thermodynamically most stable structures are shown in Fig. 11, including the ethylene binding energies (ΔE_{C2H4}) and the lowest C-H activation barrier energies (ΔE(C-H)). The ΔE_{C2H4} on pristine α-alumina was also calculated to be approximately -0.75 eV (Fig. S12). This value corresponds to the Pt-free alumina peak observed below 250 K in the experimental data. For all the stable binding modes of all three clusters, ethylene is found to bind only to Pt atoms, consistent with the interpretation of the TD-ISS results in Fig. 8. The most stable binding structures based on the GM, LM1, and LM2 isomers of each cluster are shown in Figs. S13-S15, which give both the total

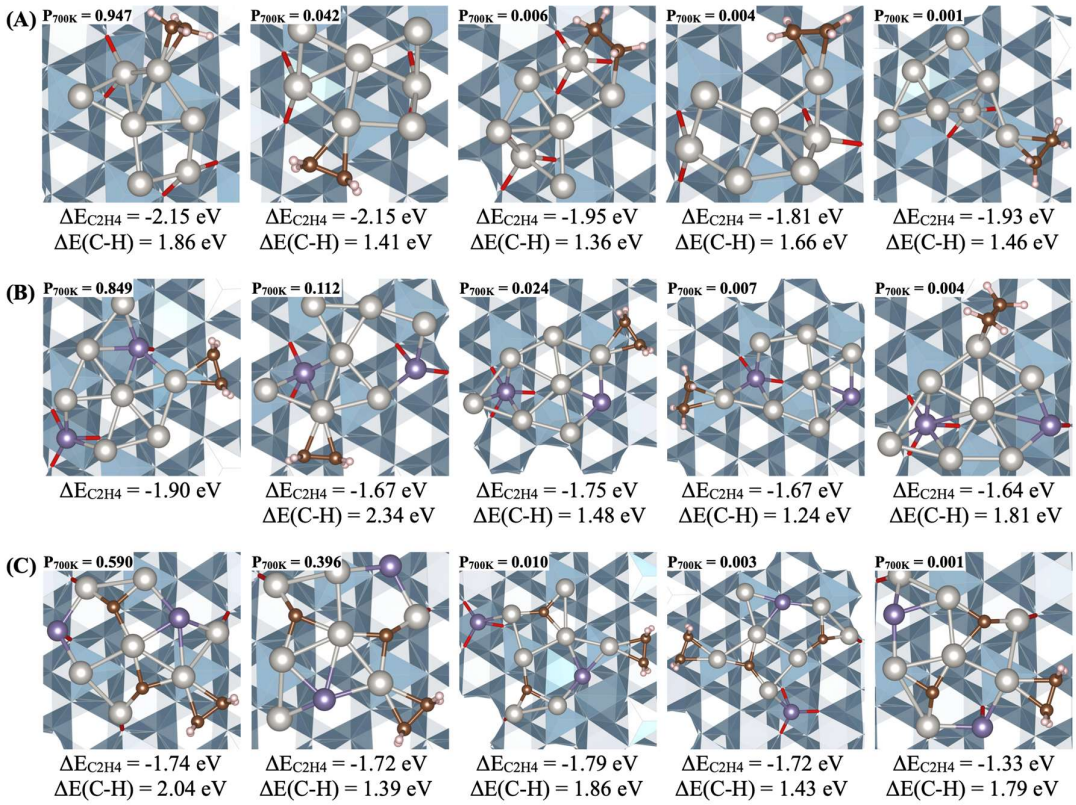

Fig. 11. Thermodynamically most stable structures of ethylene binding to (A) Pt_7, (B) Pt_7Ge_2, and (C) $Pt_7Ge_2C_2$. The ethylene binding energies (ΔE_{C2H4}), first C-H activation barriers (ΔE(C-H)), and Boltzmann population at 700 K (P_{700K}) are shown.

electronic energies relative to the GM for Pt_7-ethylene (ΔE) and the ethylene binding energies (ΔE_{C2H4}) in each structure. We note that the binding energies are electronic, rather than free energies, and therefore cannot be directly compared to the energetics estimated from TPD. However, the entropic corrections for different clusters/isomers should be similar, thus the trends of binding vs. cluster composition should be reliable.

Pt_7 binds ethylene strongly, with ΔE_{C2H4} for the most stable structures ranging from -2.15 to -1.81 eV. The most thermodynamically stable ethylene-Pt_7 structures correspond to ethylene bound to the LM1 isomer of Pt_7 (Fig. 9), aligning well with our previous findings.[13] LM1, which lies just ~0.09 eV above the prismatic Pt_7 GM, has a single-layer structure with all its Pt atoms exposed and available for adsorbate binding, while the prismatic GM structure has a central Pt atom that is caged beneath the surface layer, unable to participate in adsorbate binding. As shown in Fig. S13, ethylene binding to the GM of Pt_7 is ~0.6 eV weaker, such that the most stable such structure is nearly 0.7 eV above the most stable ethylene-LM1 structure. Indeed, even ethylene-Pt_7 structures based on the Pt_7 LM2 (ΔE = 0.15 eV) are more stable than those in which Pt_7 is assumed to retain the prismatic GM structure.

The obvious question is whether the stronger ethylene binding to the quasi-planar LM1 structure is sufficient to drive prismatic-to-quasi-planar isomerization of the cluster framework. It is not feasible to compute that barrier, however, there are several points that support the idea that ethylene-loaded Pt_7 does adopt a quasi-planar structure. Fig. 3 shows that the number of ethylene molecules that adsorb *per* Pt atom ranges from 0.53 for Pt_4 to 0.56 for Pt_7 to 0.45 for Pt_{11}, suggesting that Pt_7 exposes all Pt atoms to reactants, and only Pt_{11} retains its 3D structure when ethylene-saturated. The fact that ~4 ethylene molecules adsorb *per* Pt_7 increases the tendency to isomerize to quasi-planar structures during ethylene exposure, as we have shown previously.[13]

For Pt_7Ge_2 and $Pt_7Ge_2C_2$, the GM isomers are substantially more stable than the LM1 and LM2 isomers, and therefore dominate the cluster ensemble (P_{700K} > 98%). All Pt atoms are exposed in the cluster surface layer, and as might be expected, the thermodynamically most stable geometries with one ethylene adsorbed are all based on the GM for Pt_7Ge_2, and have all Pt atoms in the surface layer.

For ethylene-Pt_7, there are multiple low-lying configurations with di-σ ethylene binding modes that favor dehydrogenation. The branching between intact ethylene desorption vs. dehydrogenation leading to coking should be related to the relative barriers for desorption ($\Delta E(C_2H_4)$) and decomposition (ΔE(C-H)) of adsorbed ethylene,[23, 64] both shown in Fig. 11 and Figs. S16-S18. For Pt_7, the ΔE(C-H) values range from 1.86 to 1.36 eV, i.e., well below the 2.0 to 2.2 eV $\Delta E(C_2H_4)$ values, favoring decomposition over desorption, and accounting for the substantial coking and rapid deactivation observed in the ethylene TPD experiments (Fig. 1).

Experimentally, dehydrogenation leading to D_2 desorption and carbon deposition is strongly suppressed by Ge addition to the Pt_n. For ethylene-Pt_7Ge_2, the lowest energy isomer in Fig. 11 has ethylene bound to the GM isomer of Pt_7Ge_2, but despite nearly a dozen attempts starting with varying initial conditions, we were unable to locate the energy of the transition state for C-H bond activation, ΔE(C-H). The C-H scission pathway appears to involve both H migration on the cluster and restructuring of the cluster framework, i.e., the reaction coordinate appears to be quite complex. We note, however, that the next lowest energy ethylene-Pt_7Ge_2 isomer in Fig. 11 also has ethylene complexed to the GM of Pt_7Ge_2, and that isomer has ΔE(C-H) of 2.34 eV, compared to ΔE_{C2H4} of 1.67 eV, strongly favoring intact ethylene desorption over dehydrogenation. The energetics for the higher energy ethylene-Pt_7Ge_2 isomers favor intact desorption in some cases and decomposition in others, however, these isomers are high enough in energy that they are unlikely to contribute significantly in

the experimental temperature range. Other factors that should tend to promote intact desorption over dehydrogenation include the finding that Pt_7Ge_2 and $Pt_7Ge_2C_2$ predominately bind ethylene in a π-mode, which tends to favor desorption over dehydrogenation. In addition, entropic effects tend to favor desorption over decomposition because the transition states for desorption tend to be loose (low frequencies for hindered rotations and cluster-ethylene vibrations), compared to the 3- or 4-centered transition states expected for C-H bond activation (see Figs. S16-S18). Another final factor to consider is that the TPD experiments start with the clusters saturated with ethylene, and as explained above, this fact accounts for the observation that the *initial* desorption is always of intact ethylene, even for Pt_7 where C-H bond activation is strongly favored energetically. For Pt_7Ge_2, this factor presumably also favors initial intact ethylene desorption. A final point is that Ge addition is found to reduce the ethylene desorption temperatures, consistent with the lower DFT $\Delta(C_2H_4)$ values calculated for Pt_7Ge_2 compared to Pt_7.

More importantly, the analysis of ethylene binding and dehydrogenation on $Pt_7Ge_2C_2$ provides key insights into the underlying mechanism responsible for the run-to-run stability of Pt_7Ge_2. The ΔE_{C2H4} values of $Pt_7Ge_2C_2$ range from -1.79 eV to -1.33 eV, which are very similar to those of Pt_7Ge_2. The similar ethylene binding affinity between $Pt_7Ge_2C_2$ and Pt_7Ge_2, as well as their similar geometries (Fig. 9), suggests that even in the presence of small amount of coke, the Ge-doped catalyst can maintain its activity and selectivity. The ΔE(C-H) values for $Pt_7Ge_2C_2$ are also relatively high, ranging from 2.04 eV to 1.39 eV. The combined effects of its relatively weak ΔE_{C2H4} and high ΔE(C-H) values indicate a strong preference for desorption over dehydrogenation, i.e., coking might be expected to self-limit at ~2 C atoms/cluster, as is observed experimentally.

3. CO binding

Fig. 5 shows that Pt_nGe_m clusters are far more stable in repeated CO TPD runs than Pt_n clusters, preserving strong Pt-associated CO binding sites, implying that Ge addition confers stability with respect to sintering under TPD conditions. Fig. 6 shows that if the Pt_n or Pt_nGe_m are first exposed to three prior C_2D_4 TPD runs, the resulting partially coked clusters are also rather stable in repeated CO TPD runs, although only the Pt_nGe_m clusters (which would have accumulated ~2 C/cluster) retain a large high temperature CO desorption peak. To address the effects of Ge and C addition to the clusters, investigated CO binding on Pt_7, Pt_7Ge_2, and $Pt_7Ge_2C_2$ with DFT. The most energetically favorable structures and their corresponding CO binding energies, ΔE_{CO}, are shown in Fig. 12. The three most stable binding modes for the GM, LM1, and LM2 isomers of the bare clusters are shown in Figs. S19-S21. On pristine alumina the CO binding energy, ΔE_{CO}, is roughly -0.61 eV (Fig. S12). As expected, the binding strength of CO across all clusters is stronger than that of ethylene. This is consistent with the shift in the high-temperature desorption feature to higher temperatures in CO TPD (Figs. 5-6) compared to the ethylene TPD (Figs. 1-2). As expected, CO was found to bind exclusively to Pt atoms in all of the stable binding modes across all clusters.

For Pt_7, similar to the results for ethylene, CO is found to bind substantially more strongly (ΔE_{CO} = -2.83 to -2.33 eV) to cluster structures based on the single-layer LM1 isomer of Pt_7, compared to CO binding to the prismatic GM isomer (ΔE_{CO} = -2.2 to -2.1 eV), such that the lowest energy Pt_7-CO structures all have Pt_7 in a single-layer configuration. The question is whether binding CO is sufficient to drive the GM-to-single-layer isomerization, and the TPD experiments suggest that it does, at least for a saturation CO dose. This conclusion is based on the numbers of CO molecules that adsorbed *per* Pt atom in the 1st CO TPD run, which are similar for Pt_4 and Pt_7, but substantially lower for Pt_{11}. That suggests that Pt_7 adopts a single layer structure, will all Pt atoms exposed upon CO saturation, while

Pt_{11} retains its 3D structure even when CO saturated. Given the numbers of CO molecules adsorbed (~6 for Pt_7) and the high Pt-CO binding energies, isomerization to maximize the number of Pt-CO bonds is unsurprising.

For Pt_7Ge_2, the ΔE_{CO} values range from -2.62 to -2.09 eV, similar to those for Pt_7, consistent with the observation that the high T desorption peaks for Pt_n and Pt_nGe_m are similar. For $Pt_7Ge_2C_2$, the ΔE_{CO} values are smaller, ranging from -1.93 eV to -1.75 eV. We might expect, therefore, that carrying out two C_2D_4 TPD experiments to deposit carbon before measuring CO TPD would result in a noticeable decrease in the CO desorption temperature, but as noted above, roughly ~2/3^{rds} of the Pt_nGe_m clusters remain carbon free after two C_2D_4 TPD runs. The reason that C_2 addition causes a decrease in the CO affinity of Pt_7Ge_2 appears to be related to the fact that C_2 addition stabilizes the cluster framework. For Pt_7Ge_2, a noticeable restructuring of the core was observed upon CO binding, stabilizing the CO-Pt_7Ge_2 complex and enhancing the CO binding strength, however, this restructuring was not observed for $Pt_7Ge_2C_2$.

We also examined CO binding to the Pt_4-based clusters, and the results are given in Fig. S22. Experimentally, Pt_4Ge and Pt_7Ge_2 showed similar effects of Ge addition on CO TPD, i.e., the high temperature CO binding site was highly stable in repeated TPD runs, and we also observed diminished effects of adding carbon to both size PtGe clusters on the availability and strength of CO binding sites, suggesting that mechanisms are similar to those in Pt_7Ge_2. Fig. S22 shows calculated structures and binding energies for CO adsorbed at different sites on Pt_4Ge/alumina and Pt_4GeC_2/alumina, showing that CO binding remains strong after the addition of two C atoms. However, the binding strength is strongly affected by proximity to the Ge atom. The binding energies to Pt atoms that are directly bound to Ge are in the 1.14 eV to 1.58 eV range, but for Pt atoms distal to Ge, the CO binding energies are >2.5

eV, with or without added carbon atoms. The Pt atoms near Ge are generally more negatively charged in both Pt_4[23] and Pt7 (Fig. 9) based clusters. Thus, on the one hand, σ-bonding can be diminished. On the other hand, the increased negative charge could lead to enhanced π-back-donation strengthening CO binding. However, when Pt is bound to Ge in a polar covalent manner, its d-states downshift and the ability to π-back-donate is also reduced, as can be seen from the COHP analysis presented in the SI (Figs. S23-S24). In contrast, Pt atoms distal to Ge retain their original, higher d-state energetics, allowing more d-states for bonding and thus stronger π-back-donation and CO binding. In the CO TPD experiments on Pt_4Ge and coked Pt_4Ge after three C_2D_4 TPD runs, ~2 CO molecules were adsorbed *per* cluster, with desorption occurring in a broad component between 150 K and ~350 K, and in a sharp peak between with ~350 and 450 K. Assuming 1st order desorption the broad component would

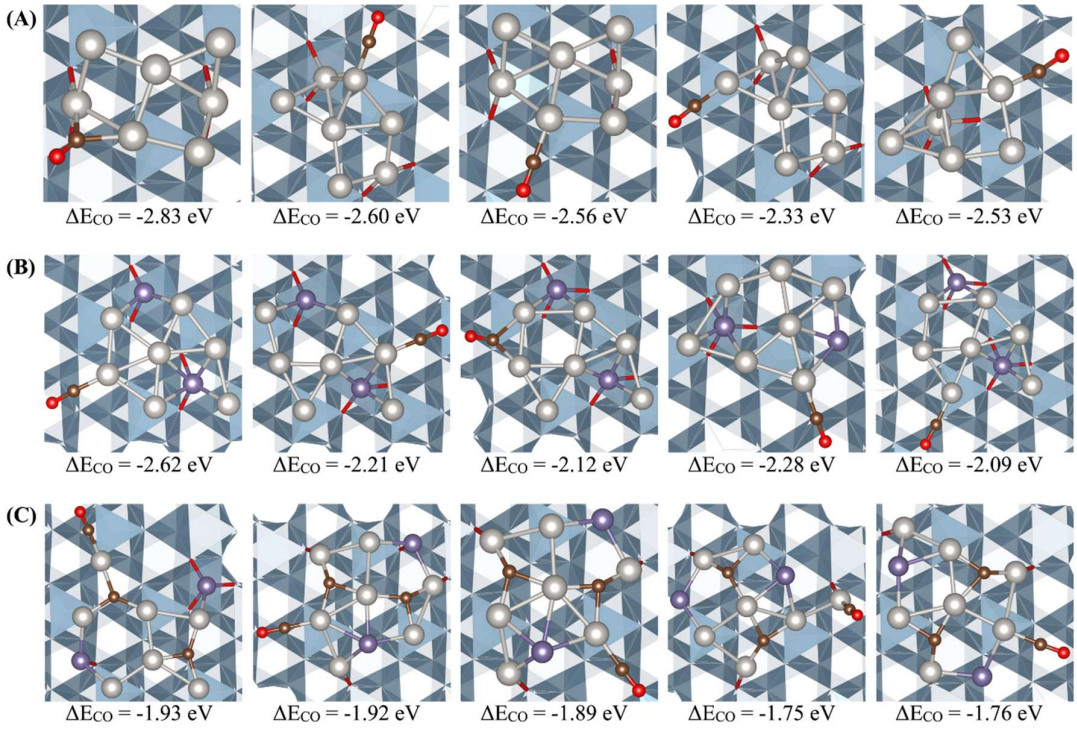

Fig. 12. Thermodynamically most stable structures of CO binding to (A) Pt_7, (B) Pt_7Ge_2, and (C) $Pt_7Ge_2C_2$. The CO binding energies (ΔE_{CO}) are shown.

correspond to desorption energies between ~0.5 and 1.1 eV, while higher temperature peak would correspond to desorption energies around 1.3 eV. Thus, while DFT appears to have significantly overestimated the CO binding energies, it suggests a tentative assignment of the low temperature desorption to CO bound to Pt atoms proximal to Ge, and the high temperature peak to CO at Pt atoms distal to Ge. This 2x scaling is attributed to the well-known CO over-binding problem in DFT,[65-67] and the lack of entropic contributions in the model.

Surprisingly, $Pt_{11}Ge_4$ was less stable than the smaller clusters in terms of the stability of strong CO binding sites, both in repeated CO TPD runs, and after three C_2D_4 TPD runs. Since all the clusters had similar Pt:Ge ratios, it is not clear why stability was lower for the largest cluster size, but unfortunately it is not feasible to attempt detailed DFT for a system with the size and complexity of $Pt_{11}Ge_4C_2$, which is expected to have a very large number of thermally accessible isomers. Note that both TPD and ISS suggest that Pt_{11} has a 3D structure, unlike the 2D structures for the smaller clusters, and both the increased Pt-Pt coordination, and reduced footprint might reduce the cluster-support binding strength, facilitating ripening at high temperatures.

III. Conclusions

We have shown that Pt_nGe_m/alumina model catalysts with different cluster sizes, and Pt:Ge stoichiometries ranging from 4:1 to ~3:1 show similar chemistry for ethylene adsorption, desorption, and dehydrogenation. Carbon deposition (coking) is substantially reduced, but not eliminated relative to Pt_n/alumina, but the numbers and strengths of strong Pt-associated binding sites are far more stable than in Pt_n/alumina. Independent of cluster size, carbon deposition in repeated C_2D_4 TPD runs on Pt_nGe_m/alumina was shown to self-limit at ~2 C atoms/cluster, i.e., coking stopped after a single ethylene decomposition event. In contrast, coking on the Pt_n/alumina reached values of roughly one C

atom/Pt *atom*, i.e., coking was not only more facile, but also increased with cluster size. CO TPD used to probe the availability of strong Pt-associated binding sites also showed that Ge addition stabilized the clusters against thermal sintering, and also against CO site blockage by carbon deposited in prior C_2D_4 TPD runs. Interestingly, the CO TPD experiments also show that for Pt_n/alumina, a small amount of carbon deposition also stabilized the clusters against sintering, but unlike Ge, did not stabilize against deactivation by additional carbon deposition. The ISS experiments showed that for Pt_n/alumina carbon initially deposits into sites on the clusters, but migrates at high temperatures such that it no longer attenuates He^+ scattering from Pt. Both the TPD and ISS experiments suggest that much of the coking-induced loss of strong Pt-associated adsorbate binding sites is the result of electronic, rather than steric effects. Ultimately, therefore, the fact that Pt_nGe_m/alumina coking self-limits at ~2 C atoms/cluster, independent of cluster size, is largely a consequence of the combined effects of Ge and C addition.

For ethylene on Pt_4Ge/alumina, DFT suggested an interesting mechanism to account for the gradual and self-limiting coking observed.[16, 23] The GM and most LM isomers were found to bind C_2D_4 in π-mode, with barriers for decomposition exceeding the energy for intact C_2D_4 desorption. The small amount of D_2 observed in the first TPD (see also Fig. 2) was attributed to a small population of a "gateway" LM isomer that supports strong di-σ ethylene bonding, favoring decomposition to produce D_2, and converting Pt_4Ge to Pt_4GeC_2, which was predicted to be stable against further coking. The continued, but slowly decreasing D_2 signal over multiple TPD runs is an effect of cluster isomerization, ensuring that the decreasing population of un-coked Pt_4Ge has a fraction with the gateway structure, resulting in additional D_2 desorption and coking, and gradually converting all the Pt_4Ge to Pt_4GeC_2. Crucially, Pt_4GeC_2 was predicted to bind ethylene strongly, explaining why desorption from strong C_2D_4 binding sites continued to be observed late in the TPD series, even after most of the original Pt_4Ge

clusters would have been converted to Pt_4GeC_2. The same effect presumably explains the persistence of strong CO binding sites after three prior C_2D_4 TPD runs. For the larger $Pt_nGe_mC_2$ clusters, the similarities in observed TPD behavior suggest that there must be considerable mechanistic similarity. Consistent with this claim, the theoretical study on Pt_7, Pt_7Ge_2, and $Pt_7Ge_2C_2$ clusters highlights the similar effects of Ge and C on the electronic properties of Pt_n, as well as the consequent impact on adsorbate binding. With a high C-H activation barrier and moderate ethylene binding strength, Pt_7Ge_2 favors desorption over dehydrogenation. Some LM isomers of Pt_7Ge_2 exhibit lower C-H activation barriers with stronger ethylene binding, acting as a precursor to the formation of $Pt_7Ge_2C_2$. The combination of a high C-H activation barrier and weak ethylene binding confers the self-limiting coking ability to $Pt_7Ge_2C_2$. Its similar ethylene and CO binding strengths to Pt_7Ge_2 contribute to the enhanced run-to-run stability of Pt_nGe_m in catalytic environments.

IV. Methods

Experimental Methods.

Sample preparation, XPS quantification, ISS and TPD procedures were performed as described previously.[16] All experimental steps were done *in situ* in a UHV system with base pressure ~1 x 10^{-10} Torr. Briefly, a Ta(110) substrate was cleaned by heating to 2100 K for 5 minutes, then alumina was deposited by evaporating Al in 5 x 10^{-6} Torr of O_2 at a surface temperature of 970 K. The alumina films were grown to a thickness of ~4 nm, as determined by XPS, based on previous work showing that for alumina films thicker than ~3 nm, the chemistry of supported clusters is thickness independent.[68] Previous work has shown that films grown under these conditions have hexagonal symmetry,[55, 56] ISS showed no evidence of surface Ta for alumina films in this thickness range on Ta(110),[57] and CO TPD (Fig. 5) from the alumina and Ge/alumina films showed no evidence of the strong

binding sites expected for Ta.[69] Thus we conclude that the alumina films are solid, exposing only Al and O binding sites.

Pt_n/alumina samples were prepared by depositing mass-selected Pt_n^+ on the alumina support at an energy 1 eV/atom, monitoring and controlling the deposition via the neutralization current. All samples contained the same total number of Pt atoms (equivalent to 10% of a close-packed Pt monolayer), differing only in the size of clusters deposited. To minimize adventitious adsorption on the samples during the initial sample holder cool-down process, the alumina films were briefly flashed to 750 K, and cluster deposition was started as the sample cooled below 300 K. TPD or other experimental steps were then carried out immediately after deposition was completed.

Pt_nGe_x/alumina samples were prepared by exposing freshly deposited size-selected Pt_n/alumina samples to 60 L of $GeCl_4$ vapor at 300 K, followed by a 300 K 6000 L exposure to H_2, resulting in HCl desorption. To avoid contaminating the UHV chamber, both alumina growth and $GeCl_4/H_2$ exposures were carried out with the sample sealed into a separately pumped UHV antechamber. Following the H_2 exposure, the Pt_nGe_x clusters are saturated with H_{ads} and have some residual Cl coverage, thus the final step was to ramp the sample temperature to 750 K, desorbing HCl and H_2.

An important point is that the Ge addition process is self-limiting, i.e., if the $GeCl_4$ dose was doubled, the amount of Ge deposited on the clusters did not change, within the uncertainty of the XPS analysis. Thus, the amount of Ge deposited is assumed to be limited by the number of $GeCl_4$ binding sites, rather than the dose. This is important, because it suggests that for samples containing a particular size Pt_n cluster, the process prepares Pt_nGe_m/alumina model catalysts with Pt:Ge stoichiometry controlled by the number of $GeCl_4$ binding sites/cluster, i.e., the cluster size and composition should be uniform.

Characterization of the Pt_nGe_m/alumna samples is discussed in the SI, along with the XPS data used to quantify the Pt:Ge stoichiometry (Fig. S25). The main conclusions from that analysis are as follows: For a Pt-free sample of the alumina thin film support, 5.9 x 10^{13} Ge atoms/cm^2 were deposited, corresponding to ~2% of the atoms in the alumina surface layer. The low Ge/alumina coverage suggests that $GeCl_4$ chemisorbed only at a small number of defects in the alumina film. Subtracting the amount of non-specific Ge deposition on alumina, resulted in estimation of the Pt_nGe_m cluster stoichiometries ranging from Pt_4Ge_1 to Pt_7Ge_2 to $Pt_{11}Ge_4$. Note that these stoichiometries were calculated assuming that the presence of ~0.1 ML equivalent of Pt on the Pt_n/alumina samples did not significantly affect deposition of Ge at alumina sites.

Ethylene TPD experiments were done by exposing a sample to 10 L of C_2D_4 at 150 K, chosen to saturate Pt-associated binding sites, while minimizing adsorption on the alumina support. The sample was then moved to within 0.5 mm of the skimmer cone aperture separating the main UHV chamber from a separately pumped chamber containing a quadrupole mass spectrometer. The sample was heated at 3 K/sec while monitoring masses of interest, including $C_2D_4^+$ and D_2^+, as well as potential adventitious species including CO^+ and H_2O^+. Repeated TPD runs, with 150 K ethylene exposures prior to each heat ramp, were done to assess how the cluster samples were changed by the TPD process.

During the first TPD runs on the Pt_n/alumina samples, significant H_2O^+ desorption signal was observed due to adsorption of background water during the cluster deposition process, however, the water signals from Pt_n/alumina and Pt-free alumina samples were nearly identical, implying that the adventitious water was mostly adsorbed on the alumina support, and thus should not have significantly affected C_2D_4 adsorption on the clusters. Adventitious CO ($P_{CO} \approx 4 \times 10^{-11}$ Torr) is potentially more problematic, because CO binding strongly to Pt. The deposition times were kept short enough to

minimize competition between adventitious CO and C_2D_4 for cluster binding sites during the 1st TPD runs. In the 2nd and subsequent TPD runs on each sample, the adventitious water and CO coverages were negligible because the inter-run time scale was short.

The calibration procedure relating $C_2D_4^+$ and D_2^+ signals to the numbers of desorbing C_2D_4 and D_2 molecules has been discussed previously.[68, 70] In essence, we measure the $C_2D_4^+$ or D_2^+ signals while leaking C_2D_4 or D_2 into the main UHV chamber at known pressures, thus creating known fluxes of C_2D_4 or D_2 effusing through the differential pumping aperture into the mass spectrometer ion source. The precision of the calibration for comparing results for different TPD runs or different cluster sizes was estimated to be on the order of ~10%, however, because of possible differences in angular and velocity distributions and detection efficiencies for effusing vs. desorbing molecules, we estimate that the absolute values are good to only ~50%.

Because CO binds strongly to Pt, it is a useful probe of accessible Pt binding sites and how they evolve as the clusters are modified by C_2D_4 TPD. Thus we also carried out CO TPD experiments with, and without prior C_2D_4 TPD runs. The ethylene TPD runs were done as described above. The CO TPD was done by dosing the samples with 10 L of ^{13}CO at 150 K, then monitoring $^{13}CO^+$ (as well as water, ^{12}CO, etc) as the samples were ramped at 3 K/second. Approximate desorption energies were estimated by fitting the desorption temperature dependence assuming 1st order desorption kinetics with a commonly used prefactor (10^{14}) as described elsewhere.[62] These correspond to desorption enthalpies, i.e., activation enthalpies, and changing the prefactor by an order magnitude would change the extracted energy scale by 7 to 10%.

He^+ ion scattering (ISS) was used to probe the as-prepared Pt_n/alumina and Pt_nGe_x/alumina samples, and samples that had been subjected to various TPD experiments. Because ISS is a destructive

technique, the "as-prepared", "post-TPD", and other ISS experiments were all done on separate sets of samples. To compensate for any day-to-day variation in He^+ beam intensity, the Pt and Ge ISS intensities were normalized to the sum of the O, Al, Pt and Ge ISS. A series of ISS experiments was done on each sample, providing additional insight into the morphology of the samples. For adsorbate free clusters, the initial Pt ISS signal is large, and decreases slowly over time as Pt is sputtered from the surface by the 1 keV He^+ beam. If, however, adsorbates (carbon, CO, etc.) are present *on top* of the clusters, the initial Pt ISS signal is attenuated, but tends to increase during the first few ISS scans as the adsorbates sputter away, then decrease in later scans as Pt begins to sputter.[60] This procedure also allows the "as-deposited" ISS data to be corrected for attenuation from adventitious CO adsorbed during cluster deposition. In essence, the slow decrease in Pt signal observed after sputtering away the CO is extrapolated to the limit of zero He^+ exposure. For samples that had been heated (during TPD or in the final step of PtGe preparation), the adventitious CO coverages were negligible.

Temperature-dependent ISS (TD-ISS) was done by exposing a Pt_n/alumina or Pt_nGe_x/alumina sample to 10 L of C_2D_4 at 150 K, then probing with a single, low He^+ current ISS scan. Comparing the Pt (and Ge) intensities with those for adsorbate-free samples, reveals the attenuation of Pt (and Ge) ISS intensities by the adsorbed C_2D_4. Samples were then heated in 50 K steps, measuring a single ISS scan at each temperature, allowing the recovery of Pt and Ge ISS signals due to adsorbate desorption to be measured and correlated with the desorption features measured in TPD experiments.

Computational methods

Calculations on surface-supported clusters were performed using plane-wave DFT in VASP,[71] using the PBE exchange-correlation functional[11] and PAW pseudopotentials.[12] Dispersion effects were described by the DFT-D3 method.[72] Unit cells were constructed from a 5-layer 3x3 supercell of Al_2O_3

with a vacuum gap of 1 nm or more, and the lower layers of the slab were kept fixed during global optimization and subsequent adsorbate binding calculations. The plane-wave cut-off was 400 eV for structural optimizations, and Gaussian smearing with a width of 0.1 eV was used. Gamma-point sampling was used for all calculations due to the large supercell used in the study. Structural sampling was performed with our in-house code PGOPT[73] and GOCIA[74] (available with documentation on GitHub) to generate 500 chemically reasonable initial structures per cluster, which we later refined with DFT. The convergence criteria for electronic minimization and ionic optimization were 10^{-6} eV and 0.02 eV/Å, respectively. QTAIM analysis was performed using the Bader program.[75, 76]

Unique, rough binding modes of C_2H_4 and CO (20 binding modes per adsorbate for each Pt_7 isomer, 30 for Pt_7Ge_2, and 40 for $Pt_7Ge_2C_2$) for the thermally accessible structures were generated using PGOPT[73] with a bond-length distribution algorithm, which we later refined at the same DFT level as the structural optimizations to obtain the final binding modes. Transition states were calculated using the climbing-image nudged elastic band (CI-NEB) method implemented in VTST[77, 78] until the forces on all images were less than 0.03 eV/Å. Local-basis projections for bonding analysis were performed using LOBSTER.[79] The PBEvaspfit basis set was used, with basis functions *5p5d6s* for Pt, *4s4p* for Ge, *2s2p* for C and O, and *3s3p* for Al.

The details of the method were chosen to ensure maximal comparability to previous studies on related materials.[16, 23] All energies in the paper are electronic energy differences. The binding energies of ethylene and CO (E_{ads}) to the clusters (clust) were calculated based on their electronic energy differences and referenced to the gaseous state (gas) of the adsorbates, using the equation $E_{ads} = E_{clust+ads} - E_{clust} - E_{gas}$.

Acknowledgements

This work was supported by the Air Force Office of Scientific Research grant AFOSR FA9550-22-1-0381. This work used computational and storage services associated with the DOD HPC, National Energy Research Scientific Computing Center, which is supported by the Office of Science of the U.S. Department of Energy under Contract No. DE-AC02-05CH11231, and UCLA IDRE Shared Cluster Hoffman2.

ASSOCIATED CONTENT

Supporting Information

The following files are available free of charge.

PtGe SI.PDF, containing supporting data and discussion, Figures S1-S25, and Tables S1-S14

AUTHOR INFORMATION

Corresponding Author

Scott L. Anderson, Dept. of Chemistry, University of Utah, 315 S. 1400 E, Salt Lake City, UT 84112, (801)-585-7289, anderson@chem.utah.edu

Author Contributions

The manuscript was written through contributions of all authors. All authors have given approval to the final version of the manuscript. Guangjing Li, and Autumn Fuchs carried out the experiments and analysis of the experimental data. Shawn Chiu, Harry W. T. Morgan, Avital Isakov, Patricia Poths, and Zisheng Zhang carried out computational studies and contributed to development of the computational methodology. Anastassia N. Alexandrova and Scott L. Anderson supervised the work and contributed to the analysis and interpretation.

Conflicts of Interest

There are no conflicts of interest to declare.

References

(1) Zhai, H.; Alexandrova, A. N. Local Fluxionality of Surface-Deposited Cluster Catalysts: the Case of Pt_7 on Al_2O_3 *J. Phys. Chem. Lett.* **2018**, *9*, 1696-1702. DOI: 10.1021/acs.jpclett.8b00379.

(2) Zhai, H.; Alexandrova, A. N. Fluxionality of Catalytic Clusters: When It Matters and How to Address It. *ACS Catal.* **2017**, *7*, 1905-1911. DOI: 10.1021/acscatal.6b03243.

(3) Adhikari, D.; Raghavachari, K. H2S Reactivity on Oxygen-Deficient Heterotrimetallic Cores: Cluster Fluxionality Simulates Dynamic Aspects of Surface Chemical Reactions. *The Journal of Physical Chemistry A* **2016**, *120* (3), 466-472. DOI: 10.1021/acs.jpca.5b10899.

(4) Xing, X.; Li, X.; Yoon, B.; Landman, U.; Parks, J. H. Dynamic Fluxionality and Enhanced CO Adsorption in the Presence of Coadsorbed H2O on Free Gold Cluster Cations. *International Journal of Mass Spectrometry* **2015**, *377*, 393-402. DOI: https://doi.org/10.1016/j.ijms.2014.07.006.

(5) Lee, S.; Lee, B.; Seifert, S.; Winans, R. E.; Vajda, S. Fischer-Tropsch Synthesis at a Low Pressure on Subnanometer Cobalt Oxide Clusters: The Effect of Cluster Size and Support on Activity and Selectivity. *J. Phys. Chem. C.* **2015**, *119* (20), 11210-11216. DOI: 10.1021/jp512157d From American Chemical Society . All Rights Reserved. CAPLUS.

(6) Gao, M.; Lyalin, A.; Takagi, M.; Maeda, S.; Taketsugu, T. Reactivity of Gold Clusters in the Regime of Structural Fluxionality. *The Journal of Physical Chemistry C* **2015**, *119* (20), 11120-11130. DOI: 10.1021/jp511913t.

(7) Ghosh, P.; Farnesi Camellone, M.; Fabris, S. Fluxionality of Au Clusters at Ceria Surfaces during CO Oxidation: Relationships among Reactivity, Size, Cohesion, and Surface Defects from DFT

Simulations. *The Journal of Physical Chemistry Letters* **2013**, *4* (14), 2256-2263. DOI: 10.1021/jz4009079.

(8) Yang, Y.; Evans, J.; Rodriguez, J. A.; White, M. G.; Liu, P. Fundamental studies of methanol synthesis from CO2 hydrogenation on Cu(111), Cu clusters, and Cu/ZnO(0001). *Phys. Chem. Chem. Phys.* **2010**, *12* (33), 9909-9917. DOI: 10.1039/c001484b From American Chemical Society . All Rights Reserved. CAPLUS.

(9) Landman, U.; Yoon, B.; Zhang, C.; Heiz, U.; Arenz, M. Factors in Gold Nanocatalysis: Oxidation of CO in the Non-scalable Size Regime. *Top. Catal.* **2007**, *44* (1-2), 145-158.

(10) Heiz, U. Chemical and catalytic properties of size-selected clusters on surfaces. *Abstracts of Papers, 232nd ACS National Meeting, San Francisco, CA, United States, Sept. 10-14, 2006* **2006**, PHYS-294. From American Chemical Society . All Rights Reserved. CAPLUS.

(11) Perdew, J. P.; Burke, K.; Ernzerhof, M. Generalized Gradient Approximation Made Simple. *Phys. Rev. Lett.* **1996**, *77*, 3865. DOI: 10.1103/PhysRevLett.77.3865.

(12) Blöchl, P. E. Projector augmented-wave method. *Physical Review B* **1994**, *50* (24), 17953-17979. DOI: 10.1103/PhysRevB.50.17953.

(13) Baxter, E. T.; Ha, M.-A.; Alexandrova, A.; Anderson, S. L. Ethylene Dehydrogenation on $Pt_{4,7,8}$ Clusters on Al_2O_3: Strong Cluster-Size Dependence Linked to Preferred Catalyst Morphologies. *ACS Catal.* **2017**, *7*, 3322-3335. DOI: 10.1021/acscatal.7b00409.

(14) Gorey, T. J.; Zandkarimi, B.; Li, G.; Baxter, E. T.; Alexandrova, A. N.; Anderson, S. L. Coking-Resistant Sub-Nano Dehydrogenation Catalysts: Pt_nSn_x/SiO_2 (n= 4, 7). *ACS Catalysis* **2020**, *10* (8), 4543-4558.

(15) Poths, P.; Hong, Z.; Li, G.; Anderson, S. L.; Alexandrova, A. N. “Magic” sinter-resistant cluster

sizes of Ptn supported on Alumina. *The Journal of Physical Chemistry Letters* **2022**, *13* (47), 11044-11050.

(16) Poths, P.; Li, G.; Masubuchi, T.; Morgan, H. W. T.; Zhang, Z.; Alexandrova, A. N.; Anderson, S. L. Got Coke? Self-Limiting Poisoning Makes an Ultra Stable and Selective Sub-Nano Cluster Catalyst. *ACS Catalysis* **2023**, *13* (2), 1533-1544. DOI: 10.1021/acscatal.2c05634.

(17) Zandkarimi, B.; Gorey, T. J.; Li, G.; Munarriz, J.; Anderson, S. L.; Alexandrova, A. N. Alloying with Sn suppresses sintering of size-selected subnano Pt clusters on SiO2 with and without adsorbates. *Chemistry of Materials* **2020**, *32* (19), 8595-8605.

(18) Li, G.; Zandkarimi, B.; Cass, A. C.; Gorey, T. J.; Allen, B. J.; Alexandrova, A. N.; Anderson, S. L. Sn-modification of Pt_7/Alumina Model Catalysts: Suppression of Carbon Deposition and Enhanced Thermal Stability. *J. Chem. Phys.* **2020**, *152* (2), 024702. DOI: 10.1063/1.5129686.

(19) Gorey, T. J.; Zandkarimi, B.; Li, G.; Baxter, E. T.; Alexandrova, A. N.; Anderson, S. L. Preparation of Size and Composition Controlled Pt_nSn_x/SiO_2 (n = 4, 7, 24) Bimetallic Model Catalysts with Atomic Layer Deposition. *J. Phys. Chem. C.* **2019**, *123* (26), 16194-16209. DOI: 10.1021/acs.jpcc.9b02745.

(20) Baxter, E. T.; Ha, M.-A.; Cass, A. C.; Zhai, H.; Alexandrova, A. N.; Anderson, S. L. Diborane Interactions with Pt_7/alumina: Preparation of Size-Controlled Boronated Pt Model Catalysts with Improved Coking Resistance. *J. Phys. Chem. C* **2018**, *122*, 1631-1644. DOI: 10.1021/acs.jpcc.7b10423.

(21) Ha, M.-A.; Baxter, E. T.; Cass, A. C.; L.Anderson, S.; Alexandrova, A. N. Boron Switch for Selectivity of Catalytic Dehydrogenation on Size-Selected Pt Clusters on Al_2O_3. *J. Am. Chem. Soc.* **2017**, *139*, 11568-11575. DOI: 10.1021/jacs.7b05894.

(22) Jimenez-Izal, E.; Liu, J.-Y.; Alexandrova, A. Germanium as Key Dopant to Boost the Catalytic Performance of Small Platinum Clusters for Alkane Dehydrogenation. *J. Catal.* **2019**, *374*, 93-100. DOI:

10.1016/j.jcat.2019.04.034.

(23) Poths, P.; Morgan, H. W. T.; Li, G.; Fuchs, A.; Anderson, S. L.; Alexandrova, A. N. Promoter–Poison Partnership Protects Platinum Performance in Coked Cluster Catalysts. *The Journal of Physical Chemistry C* **2023**. DOI: 10.1021/acs.jpcc.3c00156.

(24) Steininger, H.; Ibach, H.; Lehwald, S. Surface Reactions of Ethylene and Oxygen on Pt(111). *Surf. Sci.* **1982**, *117* (1), 685-698. DOI: /10.1016/0039-6028(82)90549-0.

(25) Ibach, H.; Hopster, H.; Sexton, B. Analysis of surface reactions by spectroscopy of surface vibrations. *Applications of Surface Science* **1977**, *1* (1), 1-24.

(26) Berlowitz, P.; Megiris, C.; Butt, J. B.; Kung, H. H. Temperature-programmed desorption study of ethylene on a clean, a hydrogen-covered, and an oxygen-covered platinum(111) surface. *Langmuir* **1985**, *1* (2), 206-212. DOI: 10.1021/la00062a005.

(27) Hatzikos, G. H.; Masel, R. I. Structure Sensitivity of Ethylene Adsorption on Pt(100): Evidence for Vinylidene Formation on (1×1) Pt(100). *Surf. Sci.* **1987**, *185* (3), 479-494. DOI: 10.1016/S0039-6028(87)80172-3.

(28) Yagasaki, E.; Backman, A. L.; Masel, R. I. The Adsorption and Decomposition of Ethylene on Pt(210), (1 · 1)Pt(110) and (2 · 1)Pt(110). *Vacuum* **1990**, *41* (1), 57-59. DOI: 10.1016/0042-207X(90)90270-9.

(29) Santra, A. K.; Goodman, D. W. Catalytic oxidation of CO by platinum group metals: From ultrahigh vacuum to elevated pressures. *Electrochim. Acta* **2002**, *47* (22-23), 3595-3609.

(30) Janssens, T. V. W.; Zaera, F. The Role of Hydrogen-deuterium Exchange Reactions in the Conversion of Ethylene to Ethylidyne on Pt(111). *Surf. Sci.* **1995**, *344* (1), 77-84. DOI: 10.1016/0039-6028(95)00836-5.

(31) Kesmodel, L.; Dubois, L.; Somorjai, G. Dynamical LEED study of C 2 H 2 and C 2 H 4 chemisorption on Pt (111): evidence for the ethylidyne group. *Chem. Phys. Lett.* **1978**, *56* (2), 267-271.

(32) Starke, U.; Barbieri, A.; Materer, N.; Van Hove, M.; Somorjai, G. Ethylidyne on Pt (111): determination of adsorption site, substrate relaxation and coverage by automated tensor LEED. *Surf. Sci.* **1993**, *286* (1), 1-14.

(33) Neurock, M.; van Santen, R. A. A first principles analysis of CH bond formation in ethylene hydrogenation. *J. Phys. Chem. B* **2000**, *104* (47), 11127-11145.

(34) Anderson, A. B.; Choe, S. Ethylene Hydrogenation Mechanism on the Platinum (111) Surface: Theoretical Determination. *J. Phys. Chem.* **1989**, *93* (16), 6145-6149. DOI: 10.1021/j100353a039.

(35) Shaikhutdinov, S. K.; Frank, M.; Bäumer, M.; Jackson, S. D.; Oldman, R. J.; Hemminger, J. C.; Freund, H.-J. Effect of carbon deposits on reactivity of supported Pd model catalysts. *Catal. Lett.* **2002**, *80* (3-4), 115-122.

(36) Mohsin, S. B.; Trenary, M.; Robota, H. J. Infrared identification of the low-temperature forms of ethylene adsorbed on platinum/alumina. *J. Phys. Chem.* **1988**, *92* (18), 5229-5233. DOI: 10.1021/j100329a032.

(37) Perry, D. A.; Hemminger, J. C. σ-Bond metathesis on a surface: dehydrogenation of cyclohexane on hydrogen-saturated Pt (111). *J. Am. Chem. Soc.* **2000**, *122* (33), 8079-8080.

(38) Carlsson, A.; Madix, R. The dynamics of ethylene adsorption on Pt (111) into di-σ and π-bonded states. *J. Chem. Phys.* **2001**, *115* (17), 8074-8082.

(39) Paz-Borbón, L. O.; Hellman, A.; Thomas, J. M.; Grönbeck, H. Efficient hydrogenation over single-site bimetallic RuSn clusters. *Phys. Chem. Chem. Phys.* **2013**, *15* (24), 9694-9700.

(40) Stöhr, J.; Sette, F.; Johnson, A. L. Near-edge X-ray-absorption fine-structure studies of

chemisorbed hydrocarbons: bond lengths with a ruler. *Phys. Rev. Lett.* **1984**, *53* (17), 1684.

(41) Cesar, L. G.; Yang, C.; Lu, Z.; Ren, Y.; Zhang, G.; Miller, J. T. Identification of a Pt3Co surface intermetallic alloy in Pt–Co propane dehydrogenation catalysts. *Acs Catalysis* **2019**, *9* (6), 5231-5244.

(42) Han, Z.; Li, S.; Jiang, F.; Wang, T.; Ma, X.; Gong, J. Propane dehydrogenation over Pt–Cu bimetallic catalysts: the nature of coke deposition and the role of copper. *Nanoscale* **2014**, *6* (17), 10000-10008.

(43) Sun, G.; Zhao, Z.-J.; Mu, R.; Zha, S.; Li, L.; Chen, S.; Zang, K.; Luo, J.; Li, Z.; Purdy, S. C. Breaking the scaling relationship via thermally stable Pt/Cu single atom alloys for catalytic dehydrogenation. *Nature communications* **2018**, *9* (1), 1-9.

(44) Jablonski, E.; Castro, A.; Scelza, O.; De Miguel, S. Effect of Ga addition to Pt/Al2O3 on the activity, selectivity and deactivation in the propane dehydrogenation. *Applied Catalysis A: General* **1999**, *183* (1), 189-198.

(45) Im, J.; Choi, M. Physicochemical stabilization of Pt against sintering for a dehydrogenation catalyst with high activity, selectivity, and durability. *ACS Catalysis* **2016**, *6* (5), 2819-2826.

(46) Fan, X.; Liu, D.; Sun, X.; Yu, X.; Li, D.; Yang, Y.; Liu, H.; Diao, J.; Xie, Z.; Kong, L. Mn-doping induced changes in Pt dispersion and PtxMny alloying extent on Pt/Mn-DMSN catalyst with enhanced propane dehydrogenation stability. *Journal of catalysis* **2020**, *389*, 450-460.

(47) Pham, H. N.; Sattler, J. J.; Weckhuysen, B. M.; Datye, A. K. Role of Sn in the Regeneration of Pt/γ-Al_2O_3 Light Alkane Dehydrogenation Catalysts. *ACS Catal.* **2016**, *6* (4), 2257-2264. DOI: 10.1021/acscatal.5b02917.

(48) Lee, M.-H.; Nagaraja, B. M.; Lee, K. Y.; Jung, K.-D. Dehydrogenation of alkane to light olefin over PtSn/θ-Al2O3 catalyst: Effects of Sn loading. *Catalysis Today* **2014**, *232*, 53-62.

(49) Sun, Q.; Wang, N.; Fan, Q.; Zeng, L.; Mayoral, A.; Miao, S.; Yang, R.; Jiang, Z.; Zhou, W.; Zhang, J. Subnanometer bimetallic platinum–zinc clusters in zeolites for propane dehydrogenation. *Angewandte Chemie* **2020**, *132* (44), 19618-19627.

(50) Cybulskis, V. J.; Bukowski, B. C.; Tseng, H.-T.; Gallagher, J. R.; Wu, Z.; Wegener, E.; Kropf, A. J.; Ravel, B.; Ribeiro, F. H.; Greeley, J. Zinc promotion of platinum for catalytic light alkane dehydrogenation: Insights into geometric and electronic effects. *ACS catalysis* **2017**, *7* (6), 4173-4181.

(51) Rochlitz, L.; Searles, K.; Alfke, J.; Zemlyanov, D.; Safonova, O. V.; Copéret, C. Silica-supported, narrowly distributed, subnanometric Pt–Zn particles from single sites with high propane dehydrogenation performance. *Chemical science* **2020**, *11* (6), 1549-1555.

(52) Ozensoy, E.; Hess, C.; Goodman, D. W. Understanding the catalytic conversion of automobile exhaust emissions using model catalysts: CO + NO reaction on Pd(111). *Top. Catal.* **2004**, *28* (1-4), 13-24.

(53) Mariscal, R.; Fierro, J. L.; Yori, J. C.; Parera, J. M.; Grau, J. M. Evolution of the properties of PtGe/Al2O3 reforming catalysts with Ge content. *Applied Catalysis A: General* **2007**, *327* (2), 123-131.

(54) Ballarini, A. D.; de Miguel, S.; Castro, A.; Scelza, O. n-decane dehydrogenation on bimetallic PtSn and PtGe catalysts prepared by dip-coating. *Catalysis in Industry* **2013**, *5* (4), 283-296. DOI: 10.1134/S2070050413040028.

(55) Chen, P. J.; Goodman, D. W. Epitaxial growth of ultrathin Al_2O_3 films on Ta(110). *Surf. Sci.* **1994**, *312*, L767-L773.

(56) Wu, Y.; Garfunkel, E.; Madey, T. E. Growth of ultrathin crystalline Al2O3 films on Ru(0001) and Re(0001) surfaces. *J. Vac. Sci. Technol., A* **1996**, *14* (Copyright (C) 2012 American Chemical Society (ACS). All Rights Reserved.), 2554-2563, 10.1116/1.579981. DOI: 10.1116/1.579981.

(57) Kane, M. D.; Roberts, F. S.; Anderson, S. L. Alumina support and Pd_n cluster size effects on activity of Pd_n for catalytic oxidation of CO. *Faraday Discuss.* **2013**, *162*, 323 - 340.

(58) Lu, K.; Rye, R. Flash desorption and equilibration of H2 and D2 on single crystal surfaces of platinum. *Surface Science* **1974**, *45* (2), 677-695.

(59) Greenlief, C.; Akhter, S.; White, J. Temperature-programmed desorption study of hydrogen-deuterium exchange on platinum (111) and the role of subsurface sites. *The Journal of Physical Chemistry* **1986**, *90* (17), 4080-4083.

(60) Kaden, W. E.; Kunkel, W. A.; Roberts, F. S.; Kane, M.; Anderson, S. L. CO Adsorption and Desorption on Size-selected $Pd_n/TiO_2(110)$ Model Catalysts: Size Dependence of Binding Sites and Energies, and Support-mediated Adsorption. *J. Chem. Phys.* **2012**, *136*, 204705/204701-204705/204712, 10.1063/1.4721625. DOI: 10.1063/1.4721625.

(61) Rabalais, J. W. *Principles and Applications of Ion Scattering Spectrometry : Surface Chemical and Structural Analysis*; Wiley, 2003.

(62) Roberts, F. S.; Kane, M. D.; Baxter, E. T.; Anderson, S. L. Oxygen Activation and CO Oxidation over Size-selected Pt_n/alumina/Re(0001) Model Catalysts: Correlations with Valence Electronic Structure, Physical Structure, and Binding Sites. *Phys. Chem. Chem. Phys.* **2014**, *16*, 26443 – 26457. DOI: 10.1039/c4cp02083a.

(63) Kaden, W. E.; Kunkel, W. A.; Roberts, F. S.; Kane, M.; Anderson, S. L. Thermal and Adsorbate Effects on the Activity and Morphology of Size-selected Pd_n/TiO_2 Model Catalysts. *Surf. Sci.* **2014**, *621* (0), 40-50. DOI: 10.1016/j.susc.2013.11.002.

(64) Hauser, A. W.; Gomes, J.; Bajdich, M.; Head-Gordon, M.; Bell, A. T. Subnanometer-sized Pt/Sn alloy cluster catalysts for the dehydrogenation of linear alkanes. *Physical Chemistry Chemical Physics*

2013, *15* (47), 20727-20734, 10.1039/C3CP53796J. DOI: 10.1039/C3CP53796J.

(65) Lininger, C. N.; Gauthier, J. A.; Li, W.-L.; Rossomme, E.; Welborn, V. V.; Lin, Z.; Head-Gordon, T.; Head-Gordon, M.; Bell, A. T. Challenges for density functional theory: calculation of CO adsorption on electrocatalytically relevant metals. *Physical Chemistry Chemical Physics* **2021**, *23* (15), 9394-9406, 10.1039/D0CP03821K. DOI: 10.1039/D0CP03821K.

(66) Grinberg, I.; Yourdshahyan, Y.; Rappe, A. M. CO on Pt(111) puzzle: A possible solution. *The Journal of Chemical Physics* **2002**, *117* (5), 2264-2270. DOI: 10.1063/1.1488596 (acccessed 4/15/2024).

(67) Feibelman, P. J.; Hammer, B.; Nørskov, J. K.; Wagner, F.; Scheffler, M.; Stumpf, R.; Watwe, R.; Dumesic, J. The CO/Pt(111) Puzzle. *The Journal of Physical Chemistry B* **2001**, *105* (18), 4018-4025. DOI: 10.1021/jp002302t.

(68) Kane, M. D.; Roberts, F. S.; Anderson, S. L. Effects of Alumina Thickness on CO Oxidation Activity over Pd_{20}/Alumina/Re(0001): Correlated Effects of Alumina Electronic Properties and Pd_{20} Geometry on Activity. *J. Phys. Chem. C.* **2015**, *119*, 1359–1375. DOI: 10.1021/jp5093543.

(69) Belov, V. D.; Ustinov, Y. K.; Komar, A. P. Carbon monoxide and carbon dioxide interaction with tantalum. *Surface Science* **1978**, *72* (2), 390-404. DOI: https://doi.org/10.1016/0039-6028(78)90303-5.

(70) Kaden, W. E.; Kunkel, W. A.; Anderson, S. L. Cluster Size Effects on Sintering, CO Adsorption, and Implantation in Ir/SiO_2. *J. Chem. Phys.* **2009**, *131*, 114701, 114701-114715. DOI: 10.1063/1.3224119

(71) Kresse, G.; Furthmüller, J. Efficient Iterative Schemes for ab initio Total-energy Calculations using a Plane-wave Basis Set. *Phys. Rev. B* **1996**, *54*, 11169. DOI: 10.1103/PhysRevB.54.11169.

(72) Grimme, S.; Antony, J.; Ehrlich, S.; Krieg, H. A consistent and accurate ab initio parametrization of density functional dispersion correction (DFT-D) for the 94 elements H-Pu. *The Journal of Chemical*

Physics **2010**, *132* (15), 154104. DOI: 10.1063/1.3382344 (acccessed 4/15/2024).

(73) Zhai, H.; Alexandrova, A. N. Ensemble-Average Representation of Pt Clusters in Conditions of Catalysis Accessed through GPU Accelerated Deep Neural Network Fitting Global Optimization. *J. Chem. Theory Comput.* **2016**, *12* (12), 6213-6226. DOI: 10.1021/acs.jctc.6b00994.

(74) Zhang, Z.; Gee, W.; Lavroff, R. H.; Alexandrova, A. N. GOCIA: grand canonical Global Optimizer for Clusters, Interfaces, and Adsorbates. ChemRxiv, 2024.

(75) Bader, R. F. W. A quantum theory of molecular structure and its applications. *Chemical Reviews* **1991**, *91* (5), 893-928. DOI: 10.1021/cr00005a013.

(76) Tang, W.; Sanville, E.; Henkelman, G. A grid-based Bader analysis algorithm without lattice bias. *J. Phys.: Condens. Matter* **2009**, *21*, 084204.

(77) Sheppard, D.; Xiao, P.; Chemelewski, W.; Johnson, D. D.; Henkelman, G. A generalized solid-state nudged elastic band method. *The Journal of Chemical Physics* **2012**, *136* (7), 074103. DOI: 10.1063/1.3684549 (acccessed 11/18/2024).

(78) Henkelman, G.; Uberuaga, B. P.; Jónsson, H. A climbing image nudged elastic band method for finding saddle points and minimum energy paths. *The Journal of Chemical Physics* **2000**, *113* (22), 9901-9904. DOI: 10.1063/1.1329672 (acccessed 11/18/2024).

(79) Maintz, S.; Deringer, V. L.; Tchougréeff, A. L.; Dronskowski, R. LOBSTER: A tool to extract chemical bonding from plane-wave based DFT. *Journal of Computational Chemistry* **2016**, *37* (11), 1030-1035. DOI: https://doi.org/10.1002/jcc.24300 (acccessed 2024/11/21).